# Synthesis and characterization of metal-oxide nanoparticles/superconductor composites

by

*Farah Naeem*

A thesis submitted in partial fulfillment
of the requirement for the degree of

**MASTER OF PHILOSOPHY**

**in**

**PHYSICS**

**DEPARTMENT OF PHYSICS**

**INTERNATIONAL ISLAMIC UNIVERSITY ISLAMABAD**

**2012**

In the Name of Allāh, the Most Gracious, the Most Merciful

**Dedicated to**

**My Ammi**

## FORWARDING SHEET BY RESEARCH SUPERVISOR

The thesis entitled "Synthesis and characterization of metal-oxide nanoparticles/superconductor composites" submitted by Farah Naeem in partial fulfilment of MS degree in Physics has been completed under my guidance and supervision. I am satisfied with the quality of student's research work and allow him to submit this thesis for further process to graduate with Master of Science Degree from Department of Physics, as per IIU rules & regulation.

**Date:**_____

**Dr. Muhammad Mumtaz**
(Supervisor)
Assistant Professor (TTS)
Department of Physics
International Islamic University
Islamabad.

06/11/12

**Dr. Kashif Nadeem**
(Co-supervisor)
Assistant Professor
Department of Physics
International Islamic University
Islamabad.

## ACCEPTANCE BY THE VIVA VOCE COMMITTEE

**Title of Thesis:** "Synthesis and characterization of metal-oxide nanoparticles/superconductor composites"

**Name of Student:** Farah Naeem

**Registration No.** 39-FBAS/MSPHY/F10

Accepted by the Department of Physics, Faculty of Basic & Applied Sciences, INTERNATIONAL ISLAMIC UNIVERSITY ISLAMABAD, in partial fulfilment of the requirements for the Master of Science in Physics with specialization in Nanotechnology.

### VIVA VOCE COMMITTEE

Dr. Shahid Shaukat
Chairman
Department of Physics (PC, FBAS)
International Islamic University
Islamabad

Chairman/Director/Head

External Examiner

Supervisor

Co-supervisor

Dated:
17/09/2012

# ACKNOWLEDGEMENT

All admirations for Almighty Allah, who is our beneficent and invites us to unravel the secrets of nature.

All respects for His Holy Prophet Hazrat Muhammad (PBUH) who is forever an ivory tower for all of us.

I am thankful to my immediate supervisor **Dr. M. Mumtaz**, Assistant Professor of Physics, Department of Physics, IIU, Islamabad for his innumerable support and kind attitude and to provide all the possible facilities to carry out this research work.

I wish to express my gratitude to my co–supervisor **Dr. Kashif Nadeem**, Assistant Professor of Physics, Department of Physics, IIU, Islamabad for his precious guidance, skilled advice in completion of my research work and thesis.

I am thankful to **Dr. Shaista shehzada**, Chairperson of Physics, Department of Physics, IIU, Islamabad for her kind and supporting attitude.

I am grateful to **Dr. Nawazish Ali Khan** and his all students of Material Science Laboratory, Department of Physics, QAU, Islamabad for their supporting behavior and cooperation.

Last but not the least I would like to pay gratitude to my loving mother, sisters specially **Sumayyah** and **Sumera** and brothers whose affections and encouragement brightened my academic career.

**Farah Naeem**

# TABLE OF CONTENT

# LIST OF TABLES

# LIST OF FIGURES

# DECLERATION

I ***Farah Naeem*** **(39-FBAS/MSPHY/F10)**, student of MS Physics (session 2010-2012) hereby declared that the matter printed in the thesis titled "**Synthesis and characterization of metal-oxide nanoparticles/superconductor composites**" is my own work and has not been published or submitted as research work or thesis in any form in any other University or Institute in Pakistan or abroad.

Dated: _____

_____

Signature of Deponent

# ABSTRACT

The nanoparticles/superconductor composites have been synthesized by solid state reaction method at 860°C. The *NiO* nanoparticles have been separately synthesized by sol-gel method at 500°C. The structural and physical properties have been examined by X-ray diffraction (XRD), Scanning electron microscopy (SEM), Energy dispersive X-ray analysis (EDX),Fourier transforms infrared (FTIR) spectroscopy, Resistivity, and AC susceptibility techniques. The X-ray diffraction technique exhibits the cubic structure of*NiO*nanoparticles and tetragonal structure of $(Cu_{0.5}Tl_{0.5})Ba_2Ca_2Cu_3O_{10-\delta}$ superconductor and exhibits the CuTl-1223 as a dominant phase with small presences of CuTl -1234 phases in these samples. There is no significant change observed in lattice parameters (c and a) with increasing the concentration of nanoparticles in CuTl-1223 superconductor. The SEM technique confirms the intergranular structure of the host CuTl-1223 superconducting matrix and EDX analysis also confirms the composition of elements and major phase of CuTl-1223 with some small impurities. The FTIR spectrum shows the vibrational bonds of NiO nanoparticles between the 420-445 $cm^{-1}$. The FTIR measurement also revealed the inclusion of *NiO* nanoparticles in these composites. The zero resistivity critical temperature is found to decrease with increasing the concentration of *NiO* nanoparticles due to lowest porosity and poor grain connectivity. TheAC susceptibility measurements of composites exhibit the decrease in magnitude of diamagnetism due to presence of antiferromagnetic *NiO* nanoparticles.

# *Chapter # 1*

# Introduction

Superconductors, nanotechnology and their composites are set to insinuate its system into our life in ways that we can only envision — more possibly, in ways that we could never imagine. Superconductivity is a fascinating phenomenon in which superconducting materials extinct all electrical resistance below a critical temperature $T_c$ [1]. Nanotechnology and superconductivity establish an enormous revolution in research world, especially when they combined with each other. This chapter reflects the richness and subtleties of these fields [2, 3].

## 1.1 Superconductivity

Superconductivity is a phenomenon in which a material exhibits the zero electrical resistance at lower critical temperature $T_c$. A superconducting behavior observed only at below the critical temperature. Above $T_c$ superconducting mechanism distracted and due to change of properties, material becomes normal [4, 5]. For example, a chunk of lead or niobium behaves like a superconductor when cooled below 20 K [6].

Superconductor contains the following properties as shown in Fig. 1.1.

**a)** Lose all resistance when cooled below a critical temperature $T_c$ [7, 8].

**b)** Magnetic flux exclusion below a critical magnetic field $H_c$ [9].

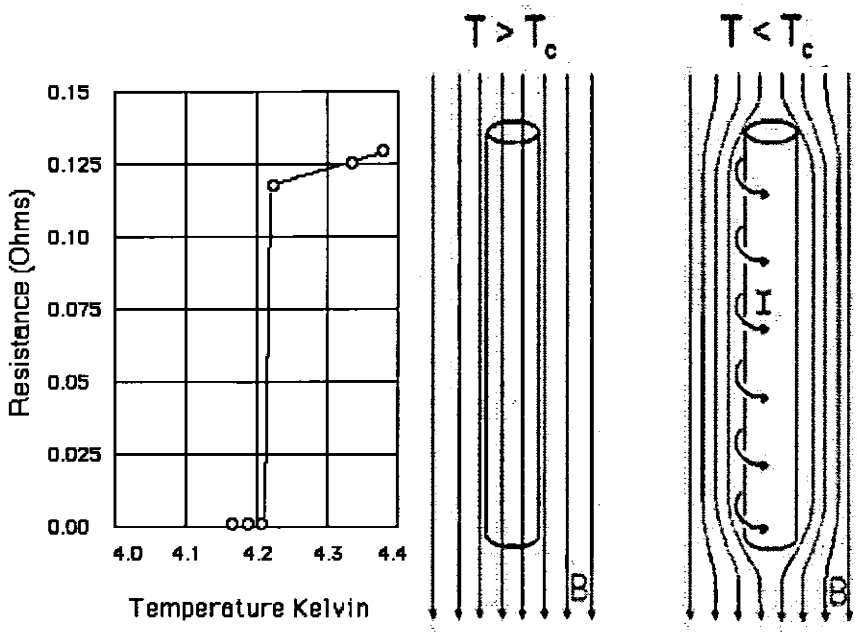


(a) (b)

**Fig. 1.1:** (a) Vanishing of electrical resistivity (b) Meissner effect [8, 1].

In 1911, Dutch Physicist H. Kamerlingh Onnes discovered the phenomenon of "superconductivity", in Kamerling Onnes' laboratory in which he described the resistance of mercury below 5K [10] and showed the sharp extinct in resistivity.He awarded the Nobel Prize in Physics in 1913 for this discovery.

Lead superconductivity at 7 K critical temperature was found in 1913 and niobium nitride superconductivity at 16 K was observed in 1941 [11].

The magnetic field repulsion from superconductor has been observed in 1933 by Meissner and Ochsenfeld in which, perfect diamagnetic behavior achieved by cancelling all magnetic fields in its interior [9].

A microscopic theory of superconductor was found in 1935 by two brothers F. London and H. London which is known as London Theory [12]. This theory showed that the Meissner effect has a significance effect on free energy of electromagnetic minimization approved by superconducting current [13].

In 1950 Ginzburg-Landau Theory of superconductivity was discovered by Landau and Ginzburg. This theory explains the phase transition from thermodynamic point and categories the superconductor into two types (Type-I and Type-II superconductor) [14].

BCS theory was found in 1957 by J. Barden, L.Cooper, and J. R. Schriffer [15]. For this discovery they were all awarded the Nobel Prize in Physics in 1972.

First commercial application (niobium-titanium alloy and superconducting wire) of superconductor was developed by researcher at Westinghouse in 1962 and in same year Josephson predicted that two pieces of superconductor which are separated by thin layer of insulator can flow super current. This miracle was known as Josephson Effect and awarded by the Nobel Prize in Physics in 1973 [16].

Bednorz and Muller discovered high $T_c$ superconductors La-Ba-Cu-O (LBCO) in 1986, which is a part of superconductivity in oxides and their transitions occurring near 30 K (Nobel Prize in Physics 1987) [17, 18]. In 1987, Lanthanum (La) replaced by Yttrium (Y) in LBCO structure and observed the critical temperature at 90 K [19].

In early 1988, BiSrCaCuO system obtained $T_c$ (R=0) around 110 K which is mixed oxide of bismuth, strontium, calcium and copper [20-22]. In TlBaCuO superconducting system different phases at different $T_c$'s around 95-105 K obtained. So

the maximum $T_c$ is found in Tl-2223 superconductor which is 127 K approximately [23-25]. Another superconductor family $Cu_{1-x}Tl_xBa_2Ca_2Cu_3O_{10-\delta}$ ($Cu_{1-x}Tl_x-1223$) has the highest $T_c$= 130 K [26]. Figure 1.2 summarizes the increase of $T_c$ with respect to time.

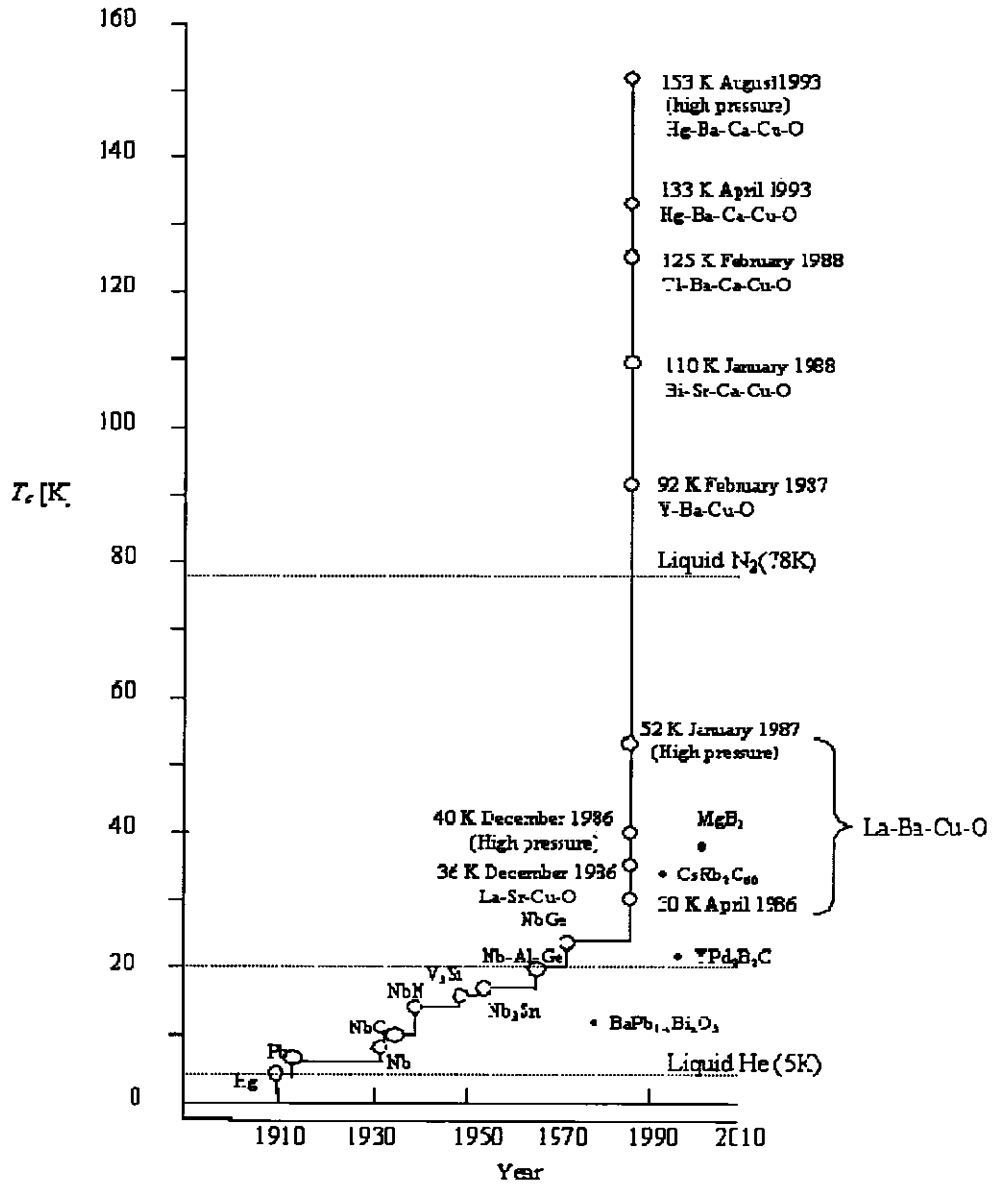


**Fig. 1.2:** Transition temperature enhancment over the years [5].

## 1.2 Classification of superconductor

A. A. Abrikosov theoretically enlightened the properties of superconductor in presence of external magnetic field. In 1957, he classified the superconductor into two types on the basis of magnetic behavior.

### 1.2.1 Type I superconductor

The process in which, complete expulsion of magnetic flux occurs below the minimum value of magnetic field $H_c$ is called critical magnetic field. At this value the specimen returns to its normal state because the magnetic field abruptly penetrates into the specimen. This type of superconductor is known as type I superconductor as shown in Fig. 1.3. Due to zero magnetic fields inside superconductor, they show the impeccable diamagnetism. At temperature less than $T_c$, it becomes linear function of applied field $H_1$. Pure metals lead and tin are type I superconductors which has low $H_c$ value. Therefore they called soft superconductors [27].

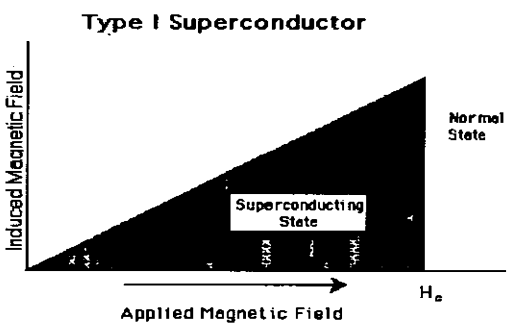


**Fig. 1.3:** Type-I superconductor [27].

## 1.2.2 Type II superconductor

Type II superconductor does not exhibit the abrupt transition change from diamagnetic state to paramagnetic state as in type-I superconductor. In type II superconductor three states exist, superconducting state, mixed state and normal state. In this type no penetration will start under the critical field $H_{c1}$ and specimen behaves as a perfect diamagnet and shows the negative magnetization.The complete flux penetration is observed into the superconducting material when the critical field $H_{c1}$ growth to reach the critical field $H_{c2}$ and at $H_{c2}$ specimen behaves as a paramagnetic with minor positive magnetization. The specimen exists on mixed state of normal state and superconducting state when partial penetration region from $H_{c1}$ to $H_{c2}$ obtained and specimen shows the partly diamagnetic behavior. This region is known as Vortex state. In this mix state partial Meissner effect is also obtained. This state magnetically as mixed state but electrically superconducting state, which shows that the penetration of magnetic field is not completely destroyed the superconductivity as shown in Fig. 1.4 [28].

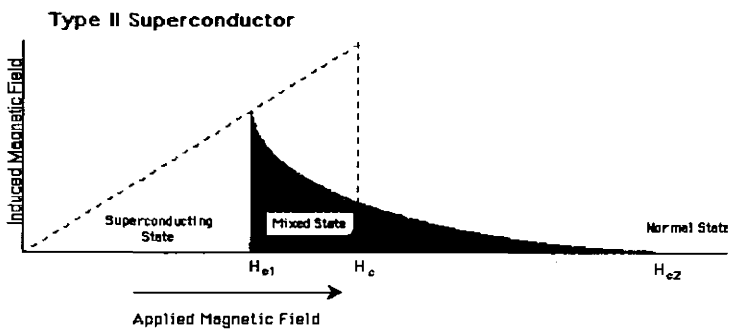


**Fig. 1.4:** Type-II superconductor [27].

## 1.3 Critical parameters

The important parameters of superconductor are critical temperature; critical magnetic field and critical current density as given below.

### 1.3.1 Critical temperature ($T_c$)

The particular temperature for superconductor at which electrical resistivity of material extinct is known as critical temperature ($T_c$) as shown in Fig. 1.5 [29].

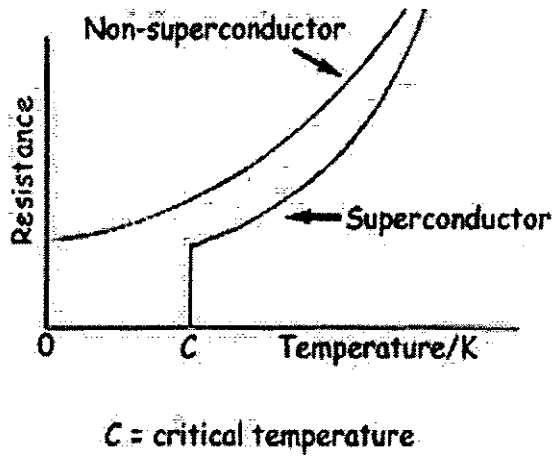


**Fig. 1.5:** Critical temperature (C) for superconductor [5].

### 1.3.2 Critical magnetic field ($H_c$)

The maximum range of magnetic field at a given temperature at which the superconductor goes to normal resistive state is known as the critical magnetic field ($H_c$). In all superconductors a particular region of temperature and magnetic field exist in which, a material contains the superconducting state. Outside this region, the material exists in normal state as shown in the Fig. 1.6 [30].

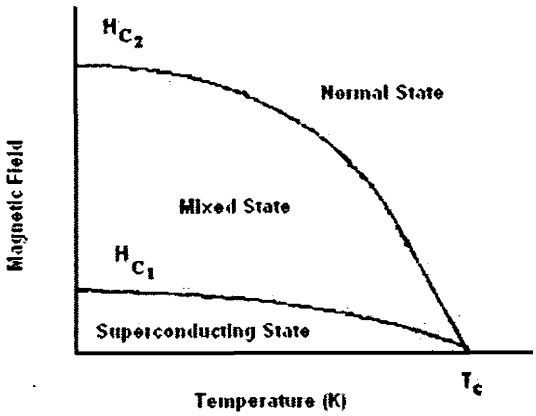


**Fig. 1.6:** Critical magnetic field in superconducting state [5].

## 1.3.3 Critical current density ($J_c$)

Due to the absence of electrical energy loss in superconductors when they carry electrical currents, relatively narrow superconducting wires can be used to carry huge currents. The passage of large amount of current through a superconductor will return back to its normal state even though it may be below its transition temperature. From the $J_c$ measurements it is clear that the superconductor will carry more current if its temperature is very low as shown in Fig. 1.7 [31].

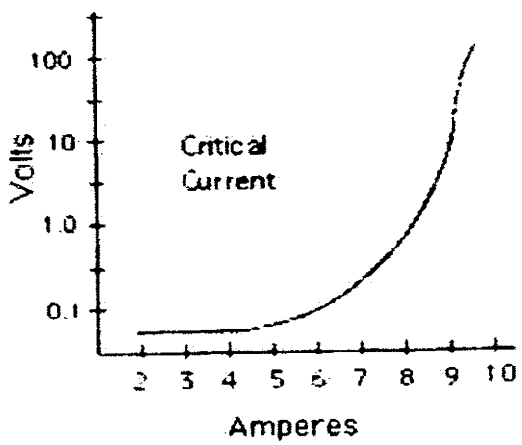


**Fig. 1.7:** Critical current density [31].

## 1.4 BCS theory

In 1957, three american Physicst Johns Bardeen, Leon Cooper and Schrieffer explained the basic mechanism of superconductors which is known as BCS Theory and awarded the Nobel Prize in Physics in 1972. This theory described the assembly of sound waves (phonon) due to lattice vibration of atoms which causes the attraction and pairing of electrons that could cross all impediments as demostrated in Fig. 1.8. This team of electron is known as Cooper pair. The Cooper pairs have net spin zero which means that Cooper pair is a Boson particle. The gathering of all particles below critical temperature in the lowest energy level is known as Boson condensation in which all the particles have same wavefunction [32]. Therefore according to BCS theory, phenomenon of superconductivity can be described as condensate of Cooper pair appeared at $T < T_c$. This shows that the dissipation free electric current is carried by Cooper pair i.e. the charge of an elementary current carrier is 2e.

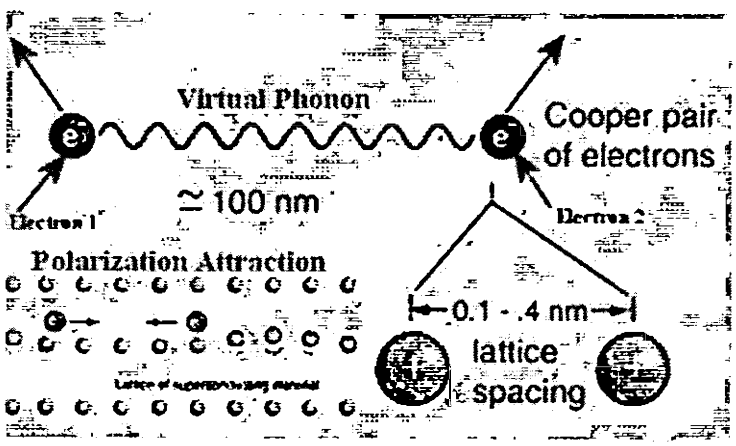


**Fig. 1.8:** Demonstration of Cooper pair electrons (BCS theory) [33].

In a superconductor the distance at which cooper pair of electrons maintains its coupled motion among the lattice point is called coherence length ξ. The shortest distance at which superconductivity may be established is $10^{-6}$m [30, 34].

## 1.5 Copper thallium (CuTl) based superconductor

Since the discovery of superconductivity, it was observed that all curprate high temperature superconductors (HTSCs) have the common structural and crystal chemical properties and have applied applications. Superconductors introduced a new subfamily CuTl-1223, based on $CuBa_2Ca_{n-1}Cu_nO_{2n+2}$ $[Cu-12(n-1)n$ (where n= 1, 2, 3...)] superconductor which has tetragonal structure [35]. It was prepared under high pressure and exhibits the better characteristics due to its high transition temperature {$T_c(0)$ ~120 K} and critical current density [35, 36-39]. This compound exhibits the least anisotropy (γ= 1.6) and long coherence length along c-axis [26, 40-41]. These parameters describe the directional dependences of the physical properties is known as anisotropy (γ) [42]. At higher pressure the synthesis of these compounds is not simple but after addition of Thallium (Tl) (act as stabilizer) in charge reservoir layer, the superconducting phase simply attained in the form of CuTl-1223 $(Cu_{1-x}Tl_x-12(n-1)n)$ superconductor, closed derivative of these compounds [43- 45]. The superconductor consists of two structural parts; one is superconductor block and second is charger reservoir block as shown in Fig. 1.9 (a). The carriers are supply by the charge reservoir layer to the plane, which are supposed to the basis of superconductivity. Figure 1.9 (b) shows the unit cell structure of CuTl-1223.

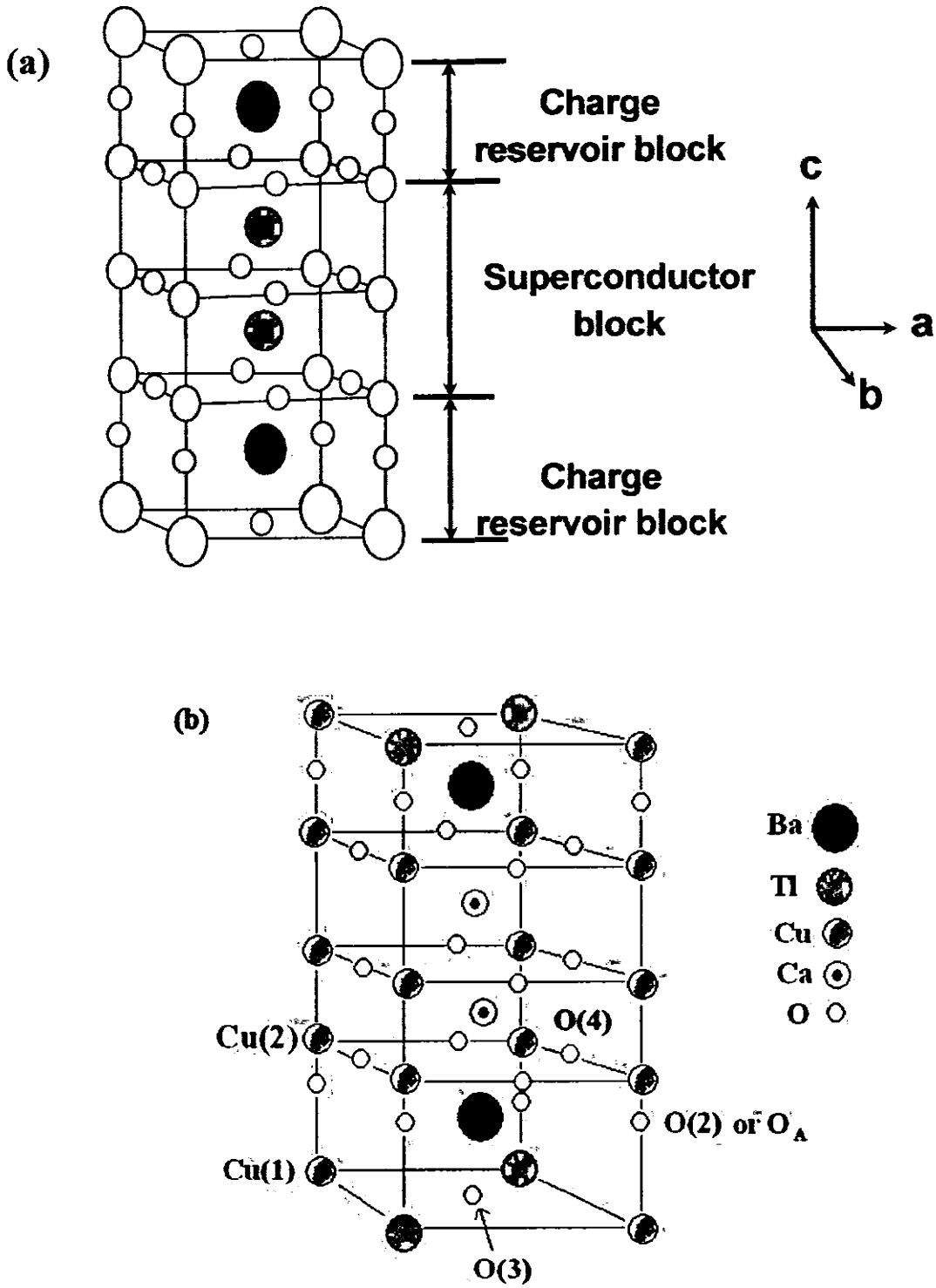


**Fig. 1.9:** (a)General crystal structure of superconductor[101], (b) Unit cell of CuTl-1223 superconductor [102].

In a unit cell of CuTl-1223 superconductor, Ba atom is used to connect the superconducting $CuO_2$ layer and detached by the two Ca atoms. This pyramid type is called the p-plane. Central or s-plane is connected by Ca atoms with outer planes. The planes which are over doped with carriers are known as p-planes while optimally doped plane is known as s-plane. In s-plane Cu atoms are called Cu(2) and oxygen atom in this plane is named as O(4). The oxygen atom connecting the $Cu_{1-x}Tl_xBa_2O_{4-\delta}$ charge reservoir layer and p-plane is apical oxygen atom is called O(2) atom which practically control the charge transport mechanism. The central oxygen atom in charge reservoir layer $Cu_{1-x}Tl_xBa_2O_{4-\delta}$ is called as $O_3$ atoms or $O_\delta$ atoms [45].

The major applications of superconductors in seven different sectors are: high engineering physics, electric powers, transportations, industrial equipment, medicines, electronics and communications, MRI (magnetic resonance imaging technique), defense and space [46].

## 1.6 Nanotechnology

Nanotechnology is an enormous scientific and rapidly change causes field which is generating new materials, devices with wide ranging applications, whose least functional range in one dimension is on nanometer scale [2, 47]. The meaning of nanotechnology varies from field to field but it is used as "catchall" description for anything very small [48].

# What is Nanoscience & Nanotechnology?

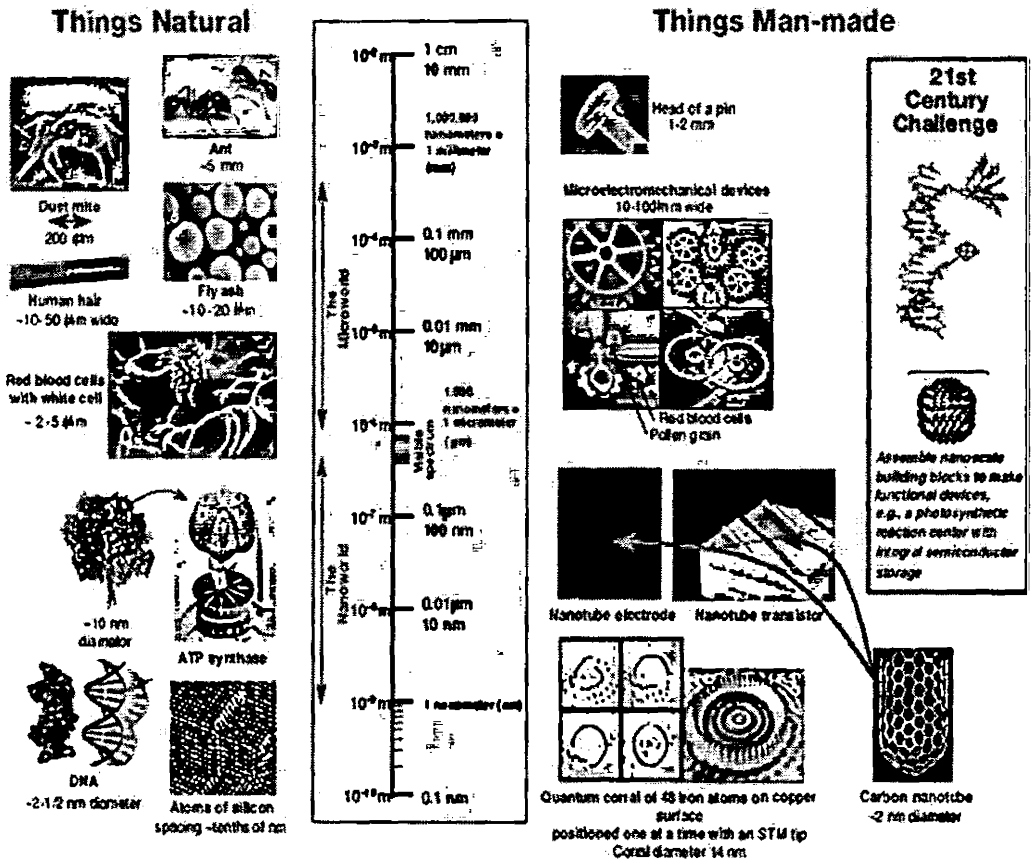


**Fig. 1.10:** Nanotechnology in different fields [49].

The size comparison from 1 cm to 1 nm between natural and artificial nanotechnology fields is shown in Fig. 1.10. A nanometer is one billionth of a meter and one meter is nearly equal to 10 hydrogen and five silicon atoms arranged in a line. Nanomaterials may be exhibit the same chemical composition but different physical properties as an equivalent to bulk material [50]. Nanotechnology is likely to increase exposure both quantitatively and qualitatively. It deals with small structures and small

sized materials. Nanomaterials due to the large surface to volume ratio show the high surface reactivity [51].

## 1.7 Nanoparticles

The particle which has less than 100 nm diameter is called nanoparticle [52, 53]. Figure 1.11 exhibits the presence of silver nanoparticles in material.

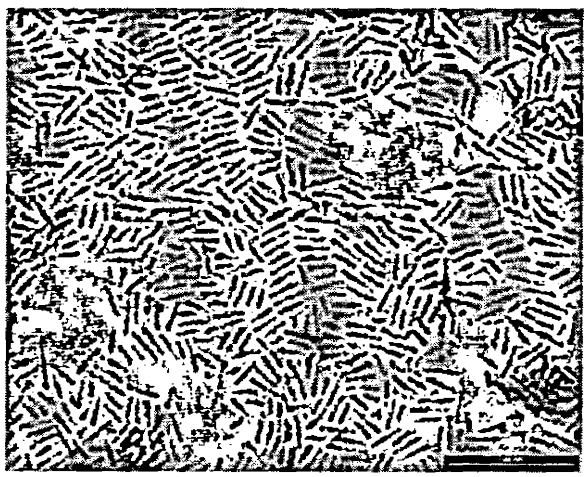

**Fig. 1.11:** TEM of silver nanoparticles [54].

Nanoparticles exhibit the new characteristics due to large surface to volume ratio and their small size invites the quantum effect to play [51]. For nanoparticle composites small size requirement is not enough. It is important to fulfill some other conditions such as, uniform size distribution, uniform shape and morphology, uniform chemical composition and crystal structure, monodispersed i.e. no agglomeration [50]. Due to these significant properties nanotechnology is motivated on different research fields, but magnetic nanoparticles are also widely used in geology, physics, medicines and

biotechnology. They produce due to interaction between particles and intrinsic properties of particles.

Nanotechnology shows an extremely wide range of favorable applications. Applications of nanotechnology depend upon the physical properties of nano-scale materials, the huge surface area and in small size nanoparticles that offers extra possibilities in multiple functions. So according to these factors nanotechnology uses in all fields such as in molecular and nanotechnology electronics devices [55], nanobots in practice of medicines [56], biological application [57], for DNA analysis [58], use the gold as catalysis [59], in engineering devices [60], to date is apply on concrete and building construction materials [48], water treatment and in soil remediation [61] and used to increase the magnetic data based storage of computer devices [62].

## 1.8 Nanoparticles/superconductor composites

Composite materials are the combination of two or more materials. Maximum composite materials contain a reinforcing material or selected filter and a compactable resin binder to gain required specific characteristics and properties. Typically the components do not dissolve in each other and can be recognized physically by interface between the components. Composite materials have been used to improve physical properties [63]. According to nanotechnology, densification of composites and polycrystalline materials can be promote by reducing a particle size, due to the large surface area and short diffusion distance [50]. The efficiency of high temperature superconductor in practical applications is often restricted due to their weak mechanical performance [64], the granularity and porous character [65], critical current density [66]

and low anisotropy [67]. After doping of different elementary particles now nanoparticles are also useful to overcome these problems from high temperature superconductors [68].

The 2009 is a very revolutionary year for composites in which some applications of cuprate superconductors are affected by the low ductility and brittleness. This occurs due to defects, surface and bulk micro cracks,voids, phase inhomogeneity and oxygen nonstochiometry [63]. This can be improved by doping of nano-$SnO_2$ which increase the volume fraction and phase without entering in phase structure and improving the microhardness of the specimen [69]. The enhancement of pinning due to 0.2 wt. % $Al_2O_3$ nanoparticles was also observed in polycrystalline (Bi-Pb)-2223 superconductors [70]. In 2010 many scientists adopted the old work and provide various new knowledge e.g. M. M. Elokret observed that by the addition of different size $ZnO$ nanoparticles in $(Cu_{0.5}Tl_{0.25}Pb_{0.25})-1223$ superconductor enhanced the critical temperature density, improved the volume fraction and reduces the grain boundaries resistance [71]. It was also observed that the Ag nanoparticles doping in $YBa_2Cu_3O_{7-\delta}$ superconductor increases the$J_c$ monotonically by increasing the particle size [72]. The microhardness of $(Cu_{0.5}Tl_{0.25}Pb_{0.25})-1223$ superconductor as the addition of nano-$SnO_2$ gradually increases and after the addition of $In_2O_3$ nanoparticles 0.1 wt. % decreases [73].

## 1.9 Motivation

CuTl-1223 superconductor has very promising applications due to its higher critical transition temperature. But the main problem of HTSCs is feeble intergrain links, structural disordness and spin-spin interaction which exhibits the depressive

superconducting properties. The metal oxide nanoparticles can play a very significant role in superconducting matrix due to their exciting physical properties as compared to their counter bulk. Therefore many scientists did work on the composites of superconductors with doping of different nanoparticles and obtained different beneficial results. In the present research work we have doped the *NiO* nanoparticles in CuTl-1223 superconductor to observe their influence on the properties of superconductor such as; critical temperature and AC susceptibility. Chapter no. 2 discusses the previous relevant work. Chapter no. 3 provides the information about synthesis and experimental techniques such as; XRD, SEM, EDX, FTIR, Resistivity and AC susceptibility. Chapter no. 4 is the most important chapter in which we discuss the obtained results. The main objective of this research is to observe the behavior of CuTl-1223 superconductor and it's above mentioned properties after doping *NiO* nanoparticles.

# *Chapter # 2*

## Review of Literature

Y. Moritomo *et al.* (1995) [74] discussed electrical resistivity and magnetic susceptibility of $La_{1-x}Sr_{1+x}MnO_4$ $(0.0 \le x \le 0.7)$ single crystal. They observed that the antiferromagnetic phase transition decreases and a spin glass phase appears for $x \ge 0.2$ due to competition between generic antiferromagnetic superexchange interaction and ferromagnetic double exchange interaction.

H. Yamauchi *et al.* (1996) [75] presented that new families of cuprate superconductors increased the No. of homologous series near to twenty. In this development, high oxygen pressure application has been used to stabilize the numerous layer structures. The cuprate structure contained the perovskite and rock-salt blocks. They observed that parent $01(n-1)$ structure series has not been superconducterized. The first member of this series is oxygen-defect $LaCuO_3$ perovskite. The 0112 structure of $BaY(Cu,Fe)O_5$ compound is the second number of this family. The third member of this homologous series is oxygen deficient $Ba_3Cu_3O_x$ triperovskite. Later due to the detection of $(Cu,C/Ba)-32(n-1)$ n series, it is possible to grow the no. of superconducting structures, besides by increasing the n value, also by making denser (increasing m) charge reservoir blocks.

V. F. Masterov *et al.* (1997) [76] showed that manganese displaces the copper atoms in $CuO_2$ planes from the BSCCO (2212) sample with composition

$Bi_2Sr_2CaCu_{2-x}Mn_xO_y$ superconductor $(x = 0, 0.8\%)$. As a result by using electron spin resonance spectroscopy a large no. of identical internal Josephson junctions and zero field oscillations of Q microwave resonator appears.

S. K. Agarwal *et al.* (1998) [77] synthesized $CuBa_2Ca_3Cu_4O_{12-\delta}$ (Cu-1234) superconductorand doped the various no. of Mg. Samples characterized by XRD, resistivity, DC susceptibility and Hall effects techniques. They observed that anisotropy was determined by the ratio of upper critical field measurement in the c-axis aligned samples with different ratios of Mg doping. They observed low anisotropy due to Mg doping in the charge reservoir blocks.

H. Ihara *et al.* (1999) [78] prepared the high $J_c$ thin films of $Cu_{1-x}Tl_x-1223$ superconductor during the investigation of high performance superconductor which based on the lowest anisotropic superconductor Cu-1234 $(CuBa_2Ca_3Cu_4O_{12-y})$ system. They observed that the high $J_c$ originated from the long coherence length along c-axis and low anisotropy of $Cu_{1-x}Tl_x-1223$ superconductor.

Tanaka *et al.* (2000) [79] synthesized the CuTl–1223 superconducting phase, annealed in nitrogen gas flow to reduce oxygen gas at 850°C for 2 h and they obtained $T_c$ = 130 K.

E. Kuzmann *et al.* (2001) [80] synthesized $(Bi_{0.93}Pb_{0.17})_2Sr_{1.9}Ca_{2.05}(Cu_{1.02}Fe_{0.01})_3O_y$ and $(Tl_{0.74}Bi_{0.25})(Ba_{0.2}Sr_{0.8})_2Ca_2(Cu_{0.99}Fe_{0.01})_3O_y$ superconductors by using Mossbauer

spectroscopy and they found that the introduction of small quantities of Fe led to a modest decrease in the critical temperatures but the samples remained superconductors.

K. Christova *et al.* (2002) [81] doped the 30-300 nm sized $MgO$ nanoparticles in Bi-2212 superconductor which did not change $T_c$ (onset) but only increased the transition sharpness and decrease the total width of the transition. These particles were incorporated inside the grains and close the grain boundary as individual particles or clusters.

S. X. Dou *et al.* (2003) [82] studied critical current effect of carbon nano-tubes by doping in $MgB_2$ superconductors. The addition of carbon nano-tubes is responsible for enhancement of flux pinning in high fields but suppressed the critical temperature.

Y. Ichiyanag *et al.* (2003) [83] discussed the magnetic properties of $NiO$ nanoparticles which were produced by annealing $Ni(OH)_2$ nano-layer, nano-cluster above 973 K in air with larger than 5.3 nm diameter. By using different samples, they studied the magnetization effect w.r.t temperature, M-H curve, ferromagnetic behavior and superparamagnetic behavior.

S. Chkoundali *et al.* (2004) [84] prepared the $NiFe_2O_4$ particles by involuntary hydrolysis of ionic iron (111) and Ni (11) solutions in 2-hydroxyethyl ether around 478 K below atomic pressure. This method improved the magnetic characteristics of obtained nanoparticles which exhibits the fine crystallinity.

S. Y. Xie *et al.* (2004) [85] synthesized the copper nanoparticles with mean diameter of 10-15 nm assembled via discharge of bulk copper rods in a celyltrimethyl

ammonium bromide acid solution. XRD results showed that prepared nanoparticles were $CuO_2$ and $CuO$ whose calculated size was nearly 10-15 nm by Sherrer's formula.

M. Ghosh *et al.* (2005) [86] formed the different size $NiO$ and $MnO$ nanoparticles by the decomposition of metal cupferronate under solvothermal conditions. They showed the increase of blocking temperature (TB) with increase of nanoparticle size but in $MnO$ exhibits the opposite behavior as compare to $NiO$ so magnetization increases with the decrease of nanoparticle size.

I. E. Agranovski *et al.* (2006) [87] prepared the Bi-2212/Ag superconducting tapes by four different methods but best result obtained by settlement method. The smooth distribution of flux pinning centers improved the tapes performance in applied magnetic field and the most important upgrading obtained in $J_c$ as compared to un-doped sample.

Q. Li *et al.* (2007) [88] formed the $NiO$ powder by sol-gel method. They obtained 13 nm single phase $NiO$ nanoparticles and observed the thin distribution and feeble agglomeration in samples.

Y. Xu *et al.* (2008) [89] discussed the $ZrO_2$and $ZnO$ nanoparticles mutually in Gd123 bulk superconductor and found $J_c$ improvement but destruction in $T_c$ due to Zn ion change in Cu site.

N. H. Mohammad *et al.* (2009) [90] described the mechanical properties of $(Cu_{0.5}Tl_{0.5})-1223$ superconductor after doping $SnO_2$ nanoparticles which were prepared by solid state reaction method. Various techniques which applied on these samples

provided different information e.g. XRD showed the increase in phase, EDS proved that $SnO_2$ does not exist in phase structure and SEM clearly examined the enhancement of microstructure density and reduction in porosity as compared to grain. They confirmed that microhardness increases due to $SnO_2$ addition.

M. M. Elokret *et al.* (2010) [91] discussed the change in $(Cu_{0.5}Tl_{0.25}Pb_{0.25})-1223$ superconductor properties due to the doping of nano- $ZnO$ nanoparticles, which were prepared by co-precipitation method. They improved the critical temperature, critical current density and enhanced phase volume fraction on different concentrations of $ZnO$ nanoparticles in bulk superconductors. They showed that low concentration of $ZnO$ nanoparticles improved the phase formation and decreased the grain boundary resistance but great concentration increases secondary phase and grain boundary resistance. The presence of Pb decreases the transition temperature, as compared to $(Cu_{0.5}Tl_{0.5})-1223$ superconductor.

M. M. Mutlagh *et al.* (2011) [92] synthesized the $Ni(OH)_2$ and $NiO$ nanoparticles. They concluded that the complexation precipitation method is low cost and high yield process, which distributed the $Ni(OH)_2$ and $NiO$ for miscellaneous homogeneities in size and shape for versatile applications.

N. A. Khan *et al.* (2012) [93] discussed the CuTl-1223 properties with doping of $CuO_2$ nanoparticles, which enhanced critical current ($T_c$), current density ($J_c$) with increasing concentration of nanoparticles.

# *Chapter #3*

# Synthesis and Experimental Techniques

## 3.1 Synthesis of superconductors

Numerous synthesis methods have been developed for the high temperature superconductors (cuprates) with the passage of time [93, 94]. The most famous method of cuprates preparation is solid state reaction method or ceramic method which has been used for the synthesis of different oxide materials [95]. In this method, it is very important to control some factors such as cation configuration, oxygen stoichiometry, cation oxidation and carrier concentration best to attain the best consequences from the characteristics of high temperature superconductors. If all materials are solid then the method is called ceramic method. The initial materials, metal oxides, carbonate nitrates or other salts after mixing heated at required temperature in sealed evacuated capsule to save from impurities. This ceramic method produced a satisfied synthesis on the basis of initial materials nature, powder mixture uniformity heating rate and as well as the reaction temperature and duration.

## 3.2 Synthesis of nanoparticles

Synthesis of nanoparticles enclosure two main approaches, top down approach and bottom up approach as shown in Fig. 3.1.

### 3.2.1 Top down approach

A method in which bulk structures are breaking down to attain a new scale structures while maintain their inherent properties without atomic level control which further distributed in different application such as, lithography, high energy ball milling, gas condensation technique and sever plastic deformation.

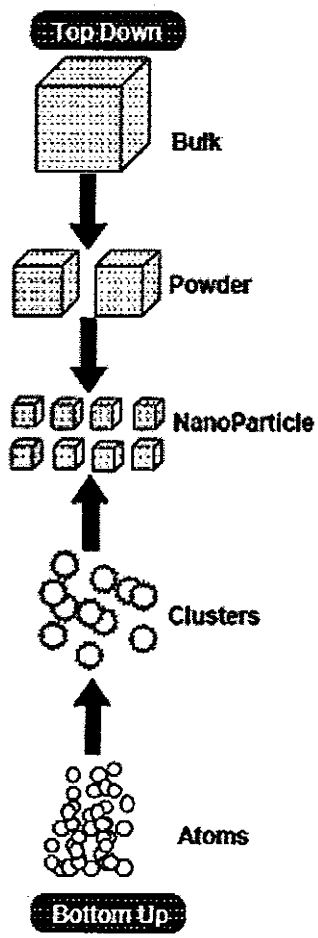


**Fig. 3.1:** Nanoparticles synthesis approach [48].

### 3.2.2 Bottom up approach

Drexler introduced the bottom up approach as molecular nanotechnology in which materials are fabricated through the process of assembly or self-assembly. It has further five branches such as, physical vapor deposition, chemical vapor Deposition, sol-gel method, self-assembly and soft lithography [48]. Among all techniques the highly pure and less surface defect technique is a wet-chemical technique which is generally used in the fields of ceramic engineeringand materials science is known sol-gel method. This technique is mainly used for the fabrication of materials (typically a metal oxide) in which a chemical solution (*sol*, short for solution) acts as the precursor for an integrated network (or *gel*) of either discrete particles or network polymers [50].

## 3.3 Synthesis of superconductors/nanoparticle composites

$Cu_{0.5}Tl_{0.5}Ba_2Ca_2Cu_3O_{10-\delta}$ bulk superconductor samples with doping of $(NiO)_y$ nanoparticles ($y = 0, 0.1, 0.2, 0.3, 0.4, 0.5, 1$ and $2\%$) were prepared by solid state reaction method. The superconductor samples were prepared by the three ways.

Firstly, the starting compounds $Cu(CN)$, $Ba(NO_3)_2$ and $Ca(NO_3)_2$ were mixed in appropriate ratios (4.845 g, 7.34 g and 2.811 g respectively) in quartz motor and pestle for about an hour in agate mortar and pestle. This material placed inside a preheated furnace at $860^0$C for 24 h and then cooled to room temperatureand added the 0.272 g $Tl_2O_3$ in this material to attain the host superconductor matrix as shown in the schematic diagram in Fig. 3.2.

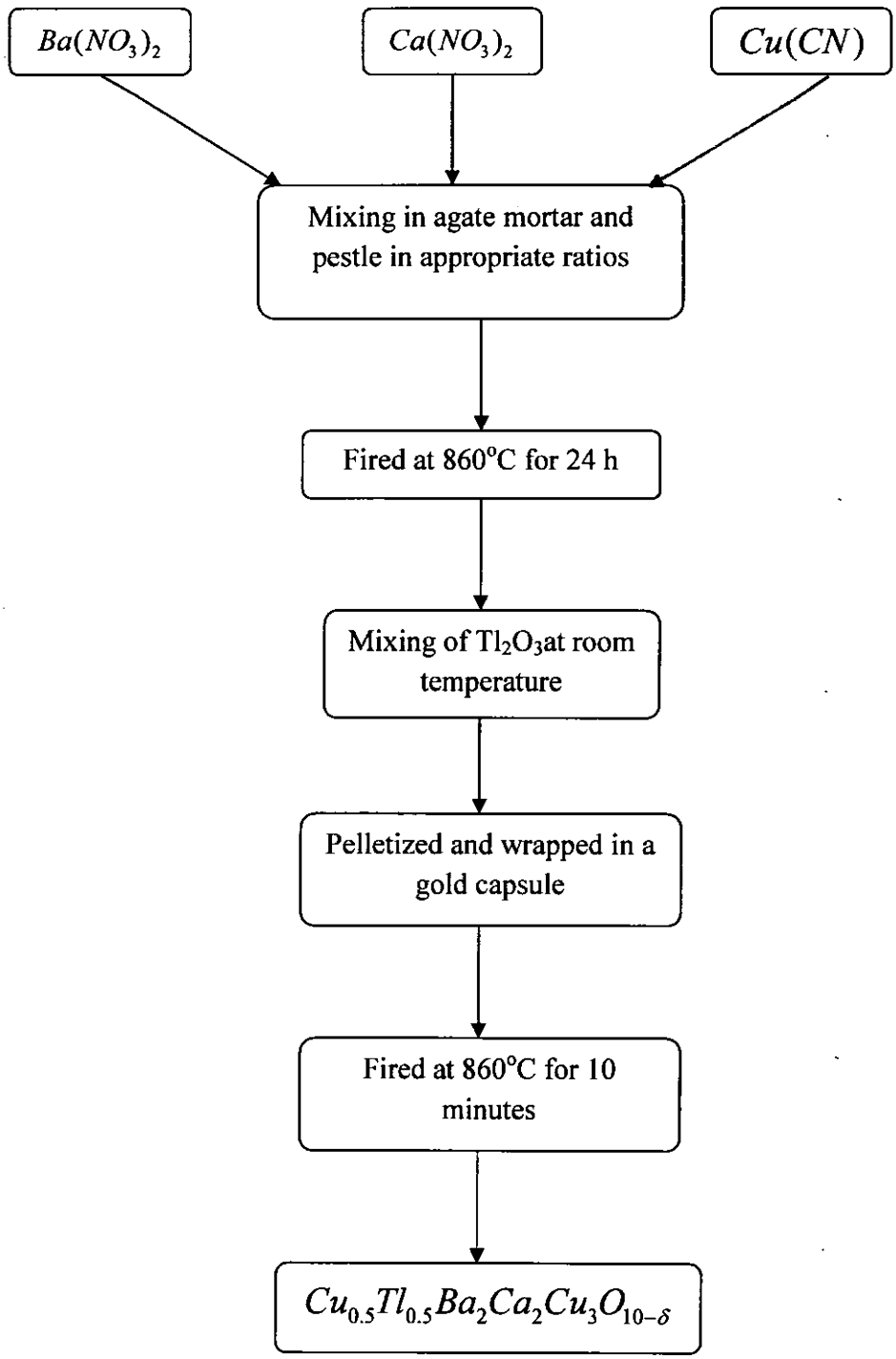


**Fig. 3.2:** Schematic diagram to synthesize $Cu_{0.5}Tl_{0.5}Ba_2Ca_2Cu_3O_{10-\delta}$ superconductor.

Secondly, the nickel oxide ($NiO$) nanoparticles were prepared by the sol-gel method as shown by schematic diagram in Fig. 3.3.

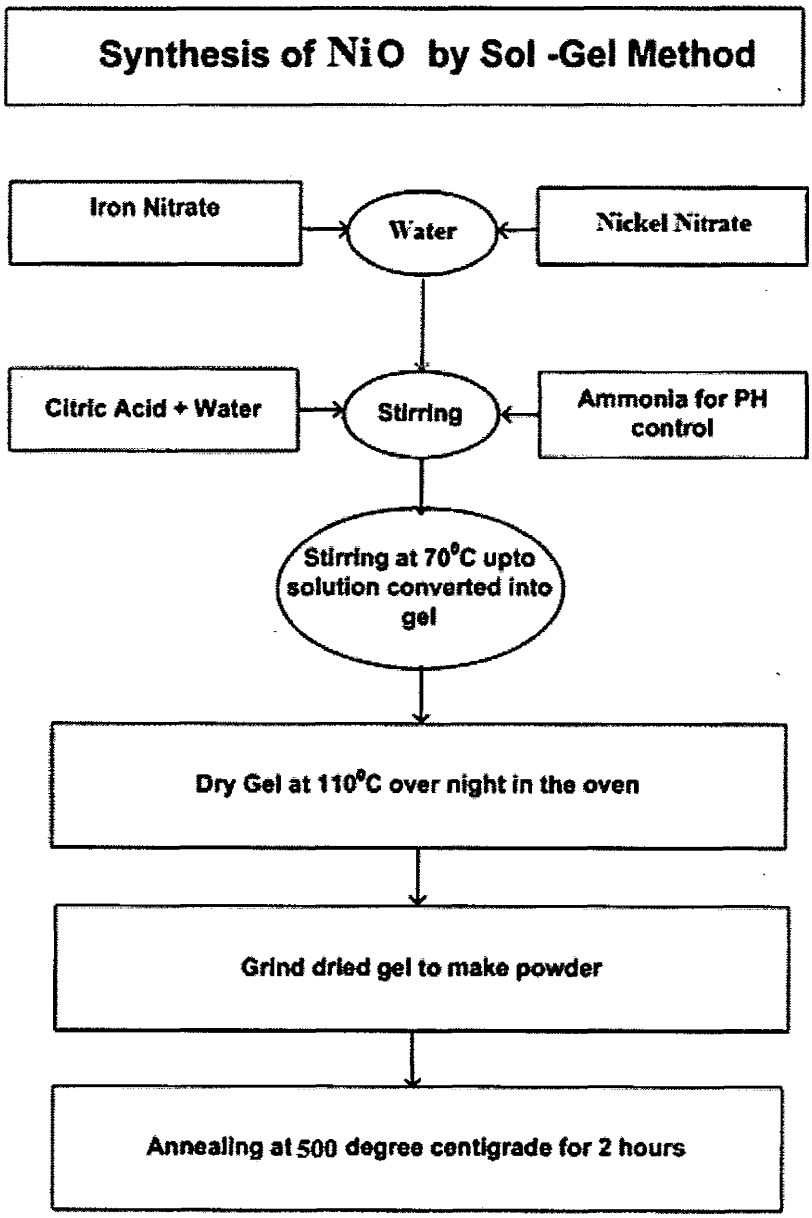


**Fig. 3.3:** Schematic diagram to synthesize $NiO$ nanoparticles.

Weight all the chemicals after appropriate calculations and then prepared the solution of the nickel nitrate and iron nitrate in the water by stirring. Likewise the solution of citric acid and water was prepared after stirring. After stirring add the solution drop by drop in to the solution of nickel nitrate and iron nitrate. The pH of solution to 5 by adding ammonia into the solution was adjusted at the end. After this, adjusted a thermometer to note the temperature we switched the hot plate. Temperature was adjusted in the range of 70-75$^0$C. After gel formation we placed the beaker in the oven to dry the gel and grinded the gel to made powder of it.

An appropriate wt. % of $NiO$ nanoparticles ($y = 0, 0.1, 0.2, 0.3, 0.4, 0.5, 1 \text{ and } 2\%$) were added in as prepared superconducting material and then ground for an hour. Thoroughly mixed material was fired at 860$^0$C for 24 h into a preheated furnace and furnace cooled to room temperature.

Thirdly, initially prepared material having both superconducting material and nanoparticles were than ground for about an hour and fired at 860$^0$C for 24 hrs. After cooling, grinding this material and intended quantity of $Tl_2O_3$ was added in this compound in appropriate ratio wt. % e.g in 0.5% is 0.109 g. The pallets were made of thoroughly thallium mixed composite under 5 tones/cm$^2$ pressures by using hydraulic press from carver. These pallets were wrapped in a gold capsules and annealed at 860$^0$C for 10 minutes in preheated furnace. Pallets were quenched to room temperature and finally we got required CuTl-based nanoparticles/superconducting composites as explain in flow chart in Fig. 3.4.

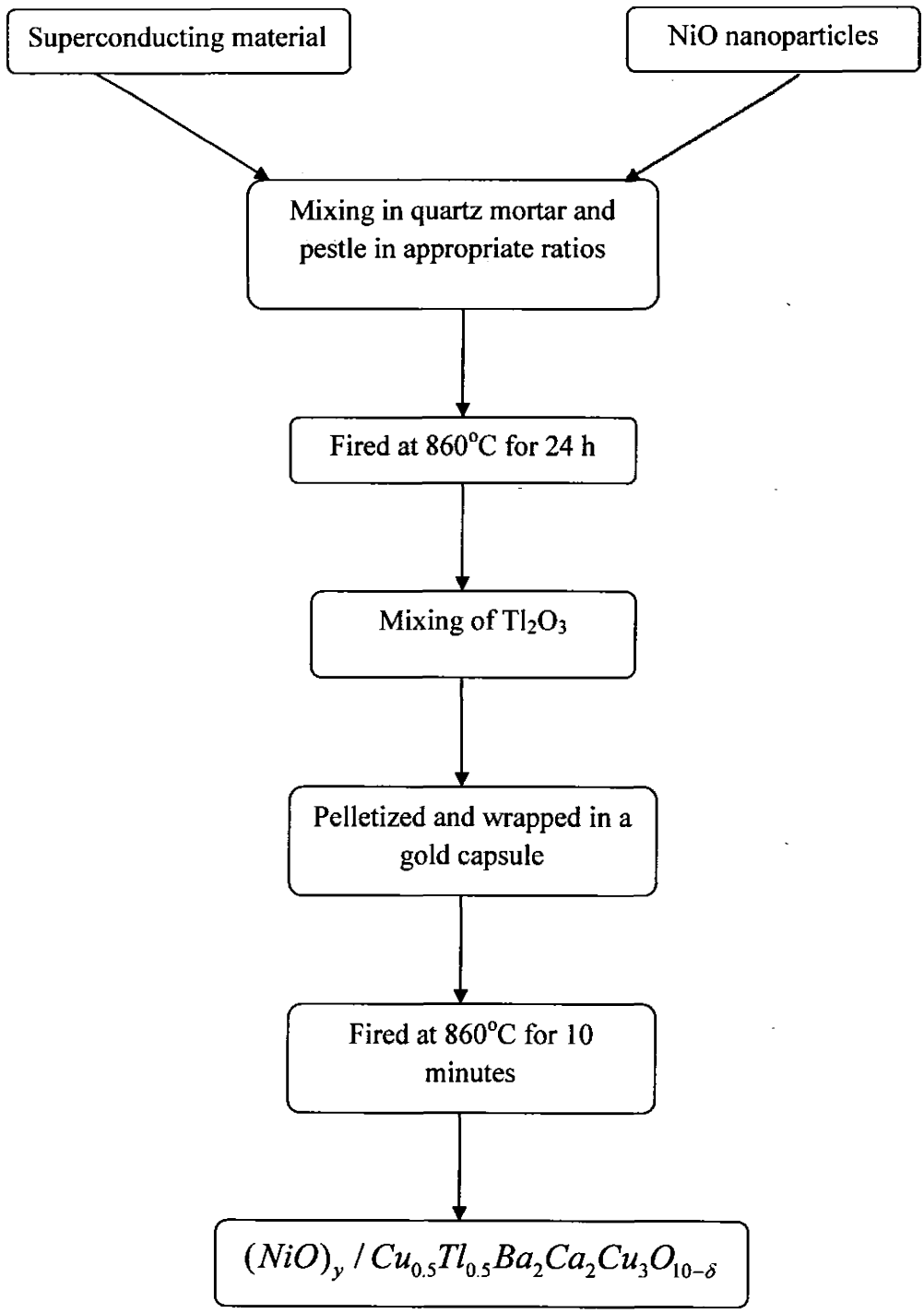


**Fig. 3.4:** Flow chart to synthesize $(NiO)_y / Cu_{0.5}Tl_{0.5}Ba_2Ca_2Cu_3O_{10-\delta}$ nanoparticles/superconductor composites.

## 3.4 Experimental techniques

The samples were characterized by the following techniques explained in sections 3.4.1 – 3.4.6.

### 3.4.1 X-ray diffraction

In research world it was assumed that a crystal consist of atoms but no one could not briefly explain the internal structure of crystal, their geometry, lattice constants defects, stress, orientation of a single crystal and identification of unknown materials [96]. With the passage of time, a new experimental technique XRD was appeared in 1912. XRD provides the complete knowledge about crystal structure of solids. X-rays generated from K-shell transition are used for diffraction analysis due to its shortest wavelength as compared to L-shell or M-shell transition. The most common target materials copper (Cu) and Molybdenum (Mo) produce X-rays with wavelength 1.54 and 0.8 Å respectively [97, 98].

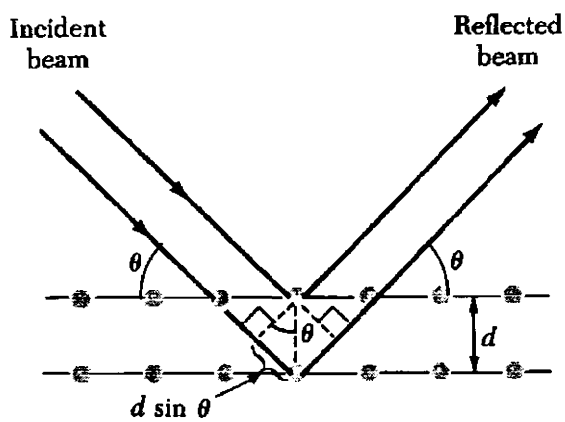


**Fig. 3.5:** X-rays diffraction [1].

A collimated beam of X-ray with wavelength 0.7 to 2 Å is incident on the specimen and Fig. 3.5 shows the diffraction phenomena by crystalline planes of specimen according to the Bragg's law.

$$2\,d\,Sin\theta = n\lambda \tag{3.1}$$

Where $n$ has integral values, $d$= spacing between atomic planes, $\lambda$= wavelength of X-ray.

Size of the unit cell can also be determined by using scherrer's formula

$$D = \frac{0.9\lambda}{\beta\cos\theta} \tag{3.2}$$

Where $D$= particle size, $\lambda$= wavelength of X-rays, $\theta$= Bragg's angle and

$\beta$= full width at half maximum of peak [99]. The schematic diagram of an X-ray diffraction is shown in Fig. 3.6.

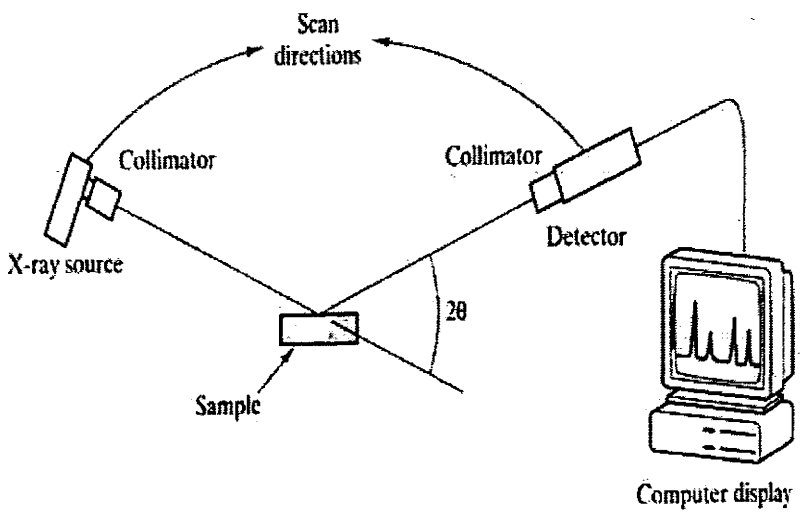


**Fig. 3.6:** X-ray diffraction system [102].

### 3.4.2 Scanning electron microscopy (SEM)

The SEM is most broadly useful technique, which gives the information about specimen morphology, chemical composition and distribution.The SEM is contrived to provide the information about the surface of the solid objects. To obtain the image from SEM use electrons instead of light. The SEM allows a big part of the sample to be in focus in one time due to its large depth of field property and produces the three dimensional image. Due to high resolution SEM provides the closed image features of a specimen and provides the crystallographic information.

An electron beam is produced by electron gun may either thermionic or field emission. This electron gun focused by condenser lenses and by using the objective lenses determined the final spot size of electron beam which scanned on the sample surface in a raster pattern in synchronization with beam in CRT as shown in Fig. 3.7. A high energy electron beam is used to excite the sample and different signals are collected for analysis so that an image can be obtained. The signals provide the topographical, chemical and crystallographic information, respectively, of specimen surface. The main applications of SEM are topography (surface analysis, hardness and reflectivity etc.), morphology (shape and size of object, strength, defects in IC and Chips etc.), composition (elements and compounds, melting point, reactivity and hardness etc.), crystallographic information (grains arrangement, conductivity, electrical properties and strength etc.) [100].

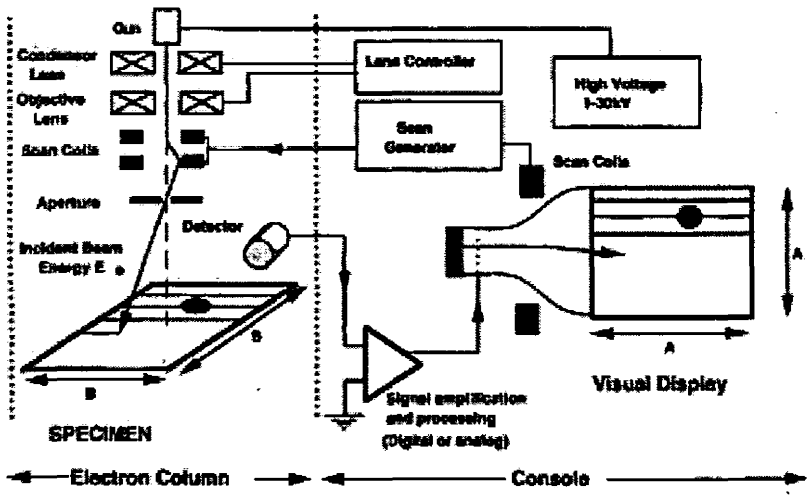


Fig.3.7: SEM schematic representation [100].

### 3.4.3 Energy dispersive X-ray analysis (EDX)

The integral feature of scanning electron microscope which is used to determine the elements of specimen is recognized as EDX (energy dispersive X-ray). In EDX technique a beam of electrons bombarded with specimen to eject some electrons out of them and produces vacancy. The outer shell electron comes to fill this vacancy and emits some amount of energy in the form of X-rays. The peaks obtained from EDX analysis linked to the different atoms of specimen which confirm the existence of different elements in specimen. The more concentrated element is in the specimen shows the higher peak in spectrum.

### 3.4.2 Scanning electron microscopy (SEM)

The SEM is most broadly useful technique, which gives the information about specimen morphology, chemical composition and distribution.The SEM is contrived to provide the information about the surface of the solid objects. To obtain the image from SEM use electrons instead of light. The SEM allows a big part of the sample to be in focus in one time due to its large depth of field property and produces the three dimensional image. Due to high resolution SEM provides the closed image features of a specimen and provides the crystallographic information.

An electron beam is produced by electron gun may either thermionic or field emission. This electron gun focused by condenser lenses and by using the objective lenses determined the final spot size of electron beam which scanned on the sample surface in a raster pattern in synchronization with beam in CRT as shown in Fig. 3.7. A high energy electron beam is used to excite the sample and different signals are collected for analysis so that an image can be obtained. The signals provide the topographical, chemical and crystallographic information, respectively, of specimen surface. The main applications of SEM are topography (surface analysis, hardness and reflectivity etc.), morphology (shape and size of object, strength, defects in IC and Chips etc.), composition (elements and compounds, melting point, reactivity and hardness etc.), crystallographic information (grains arrangement, conductivity, electrical properties and strength etc.) [100].

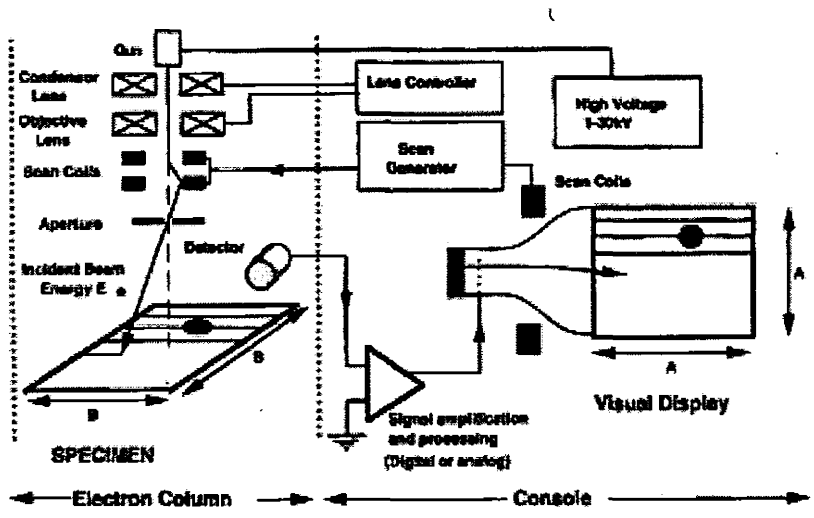


Fig.3.7: SEM schematic representation [100].

### 3.4.3 Energy dispersive X-ray analysis (EDX)

The integral feature of scanning electron microscope which is used to determine the elements of specimen is recognized as EDX (energy dispersive X-ray). In EDX technique a beam of electrons bombarded with specimen to eject some electrons out of them and produces vacancy. The outer shell electron comes to fill this vacancy and emits some amount of energy in the form of X-rays. The peaks obtained from EDX analysis linked to the different atoms of specimen which confirm the existence of different elements in specimen. The more concentrated element is in the specimen shows the higher peak in spectrum.

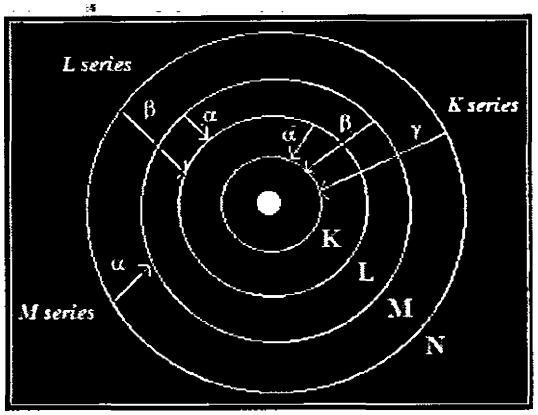


**Fig. 3.8:** Different X-rays emission in EDX process [101].

Figure 3.8 shows the transfer of electrons from L-shell and M-shell to K-shell which is known as K-Alpha peak and K-Beta peak. This mean a normal spectrum of EDX explain the relation of peaks and energy levels and exhibits the type of X-rays [101].

### 3.4.4 Fourier transforms infrared spectroscopy (FTIR)

Fourier transform infrared absorption spectroscopy technique is best method of infrared spectroscopy which is used to detect molecular vibrations. FTIR basically consists of a Michelson interferometer which can distinct the infrared radiations into its constituent wavelengths [50]. The basic diagram of Michelson interferometer is shown in Fig. 3.9.

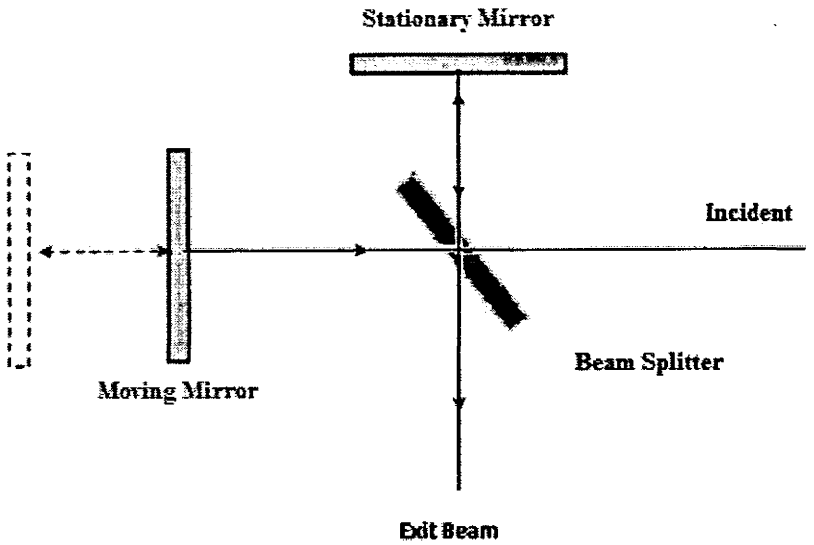


**Fig. 3.9:** Michelson interferometer [102].

The infrared radiations are used due to lattice vibrations wavelength which exists in the range of infrared region of electromagnetic spectrum. The infrared radiations will be absorbed into the sample in the result of interaction and frequency matching with molecular vibrations. In oxide superconductors it may be possible that electron-phonon interaction is the origin of superconductivity. So the infrared absorption spectroscopy is very useful to study the possible connections between lattice vibrations and superconductivity. For bulk samples, thin pallets were made by mixing a small quantity of KBr with minor quantity of sample. The background spectrum was taken with KBr pellet then sample spectrum was observed. The resolution of spectrometer is arranged within 400 to 700 $cm^{-1}$. The numbers of scans taken for sample were 10 to 50. The spectrometer subtracts the background spectrum and sample spectrum was observed.

### 3.4.5 Resistivity measurements

The resistivity technique is used to find out the critical temperature of material. We observed the behavior of superconductor before and after doping in material. The source of resistivity in materials is lattice defects, lattice vibration and electron-electron interaction [103]. The four probe method is used, in which two lead wires were used to carry the current by constant current source and two middle wires are used for voltage drop measurement. These wires are connected to the sample through the silver paint (with low contact resistance). A resistivity setup can be explained by the schematic diagram in Fig. 3.10.

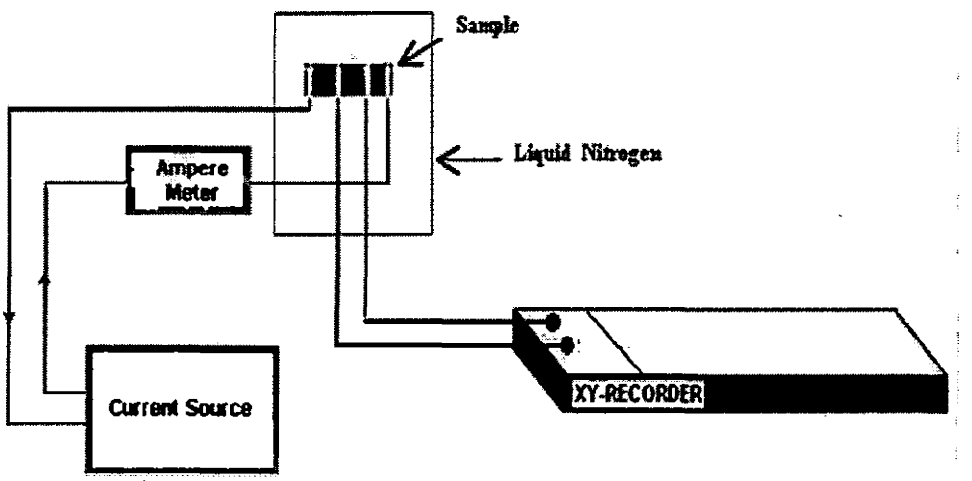


**Fig. 3.10:** Setup of resistivity measurements [102].

Resistivity can be measured by the following formula

$$\rho = \frac{V(T)A}{IL} \tag{3.3}$$

where,

$V(T)$= Voltage drop across the sample, $A$= Cross-sectional area of the sample, $L$ = Length of the sample and $I$ = Current through the sample.

A liquid nitrogen dewer was used as a cryostat for the measurement of resistivity which is dependent on temperature. The resistivity measurement of a superconducting sample was carried out during heating the sample from 77 K to room temperature.

### 3.4.6 AC susceptibility measurements

When a magnetic field is applied on a superconducting sample, it magnetized and change behavior is observed. This change behavior is known as susceptibility. It is denoted by $\chi$ the fundamental susceptibility. This fundamental susceptibility is divided into two terms, DC susceptibility and AC susceptibility [104].

If DC magnetic field is applied on sample without produced change in magnetic moment w.r.t time is known as DC susceptibility and can be explain as

$$\chi_{dc} = \frac{M}{H_{dc}} \tag{3.4}$$

where,

$M$ is the magnetization of the material and $H$ is the applied field.

In AC susceptibility, AC magnetic field is applied on the sample and produced change w.r.t time and gives the following expression.

$$\chi_{ac} = \frac{dM}{dH_{ac}} \tag{3.5}$$

It has two important components, in-phase susceptibility '$\chi'$' and out-phase susceptibility '$\chi''$'as shown in Fig. 3.10.

$$\chi = \chi' + i\chi''$$

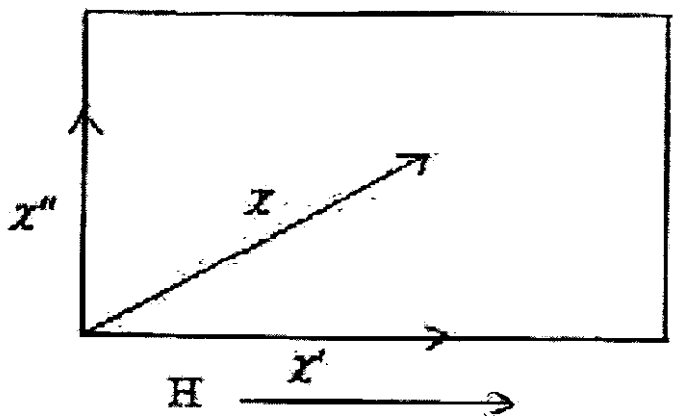


**Fig. 3.11:** In phase and out of phase part of susceptibility [101].

The real part of AC susceptibility describes the magnetic response of the system andthe correlation among the magnetic spins clusters. It informs about dislocations, transition temperature which present in different magnetic materials. The imaginary part is out of phase shows the inability of system to follow the variations of system in applied magnetic field entirely in coherence or in phase with it and also displays the energy dissipation in the magnetic system. The AC susceptibility techniques used to discuss the filamentary superconductivity, surface barrier, and the effect of granularity [105]. Figure 3.12 explains the schematic diagram of the AC susceptibility. AC susceptibility apparatus consist of a primary coil and a secondary coil which wound on a non-magnetic holder. The two secondary coils were used to determine the magnetic behavior of a sample. Superconductor sample was placed in one of the secondary coil and cooled below the critical temperature.

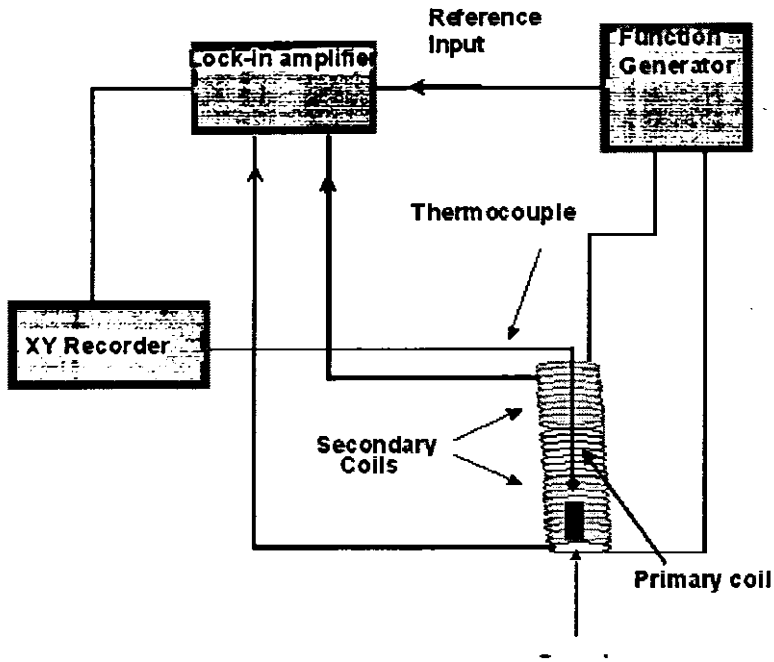


**Fig. 3.12:** Setup of AC susceptibility measurements [102].

Signal was obtained due to voltage difference between two coils. In AC susceptibility apparatus, primary coil and a secondary coil were wound by using copper wire. The sample was positioned in the lower secondary coil and cooled down to the 77 K in liquid nitrogen dewer. A T-Type thermocouple was adjusted in the intermediate vicinity of sample for temperature measurements. Sample was applied one volt signal at 270 Hz from a function generator "Model HP 3314 A" and used lock in amplifier "Model SR 530" for amplification. The critical temperature value was affected by increasing or decreasing frequency value. The susceptibility graph was plotted on XY-recorder.

# *Chapter # 4*

# Results and Discussion

## 4.1 Introduction

The $Cu_{0.5}Tl_{0.5}Ba_2Ca_{n-1}Cu_nO_{2n+4-\delta}[Cu-12(n-1)n]$; n = 2, 3, 4... (CuTl-1223) is one of the most fascinating and promising family of high temperature superconductors (HTSCs) due to low anisotropy ($\gamma$= 5) and long coherence length along c-axis [106] which has a charge reservoir layer $Cu_{0.5}Tl_{0.5}Ba_2O_{4-\delta}$ and three $CuO_2$ conducting planes [107]. It is observed that the concentration of carriers in $CuO_2$ planes is controlled by the addition or elimination of oxygen in charge reservoir layer. The doping of impurity in HTSCs is affected the superconductivity due to different electronic configuration of doped atoms and interaction with free carriers [108, 109]. Doping materials can be enhancing the superconducting properties but in some opinions, doping of small quantity can damage the large portion of superconductivity [110]. Therefore we try to investigate the nanoparticles doping effect on superconducting properties which provides the different results. Nanoparticles doping has affected on the flux pinning. It was observed that the flux pinning of $MgB_2$ superconductor enhanced by the doping of $SiC$ nanoparticles and it was noticed that $T_c$ of $MgB_2$ bulk superconductor decreases with carbon doping [111]. The $Al_2O_3$ nanoparticle substitution affected the (Bi, Pb)-2223 superconducting properties. It observed that the large quantity of $Al_2O_3$ nanoparticles decrease the critical current density ($J_c$) and critical temperature ($T_c$) [112]. The change in

superconducting properties of $MgB_2$ superconductor after addition of Fe nanoparticles decreases the $T_c$ and $J_c$ due to their high reactivity [113]. The improvement of $J_c$ and $T_c$ in Bi-2212/Ag superconductor tapes was observed by the substitution of $MgO$ nanoparticles [86]. The enhancement in normal core pinning of Gd-123 superconductor was observed with the addition of $ZrO_2$ nanoparticles [114] and $ZnO$ nanoparticles addition can also increase the $J_c$ of Gd-123 bulk superconductors [115]. The $MgO$ nano-oxides addition in small quantity enhanced the grain connectivity; critical current and microhardness of $(Cu_{0.5}Tl_{0.75})-1234$ superconductor phase but decrease the above mentioned properties by adding in large quantity [89]. The microhardness of $Cu_{0.5}Tl_{0.5}-1223$ superconductor enhanced with the addition of $SnO_2$ nanoparticles and vanishing the grains porosity [116]. The doping of Zn in CuTl-1223 superconductor investigated the reduction of antiferromagnetism due to increase of carrier's density in conducting planes [90]. The microstructure mechanical property of $Cu_{0.5}Tl_{0.5}-1223$ superconductor is affected by the doping of $SnO_2$ and $In_2O_3$ nanoparticles. As the $SnO_2$ nanoparticles doping gradually increases the microhardness of $Cu_{0.5}Tl_{0.5}-1223$ superconductor and same results obtained at 0.1% addition of $In_2O_3$ but after this range $In_2O_3$ exhibits the depression inmicrohardness property [73]. The enhancement of the volume fraction and phase improvement of $Cu_{0.5}Tl_{0.25}Pb_{0.25}-1223$ superconductor is obtained by doping of $ZnO$ nanoparticles at low concentrations [72]. The substitution of Ag nanoparticles in $YBa_2Cu_3O_{7-\delta}$ bulk superconductor enhanced the critical current density and grains connectivity [15]. The doping of $NiO$ nanoparticles in Bi-Sr-Ca-Cu-O

superconductor depressed the $T_c$ and $J_c$ due to the enhancement of disorientation of grains and agglomeration of nanoparticles in grain boundaries [117].

We have studied the superconducting properties of superconductor $Cu_{0.5}Tl_{0.5}Ba_2Ca_2Cu_3O_{10-\delta}\,(CuTl-1223)$ and $(NiO)_y / Cu_{0.5}Tl_{0.5}Ba_2Ca_2Cu_3O_{10-\delta}$ composite which are prepared by the doping of NiO nanoparticles by using solid state reaction method at $860^0$C in different compositions such as y = 0, 0.1, 0.2, 0.3, 0.4, 0.5, 1 and 2%. These superconductor samples have extensively characterized by the following techniques.

## 4.2 X-ray diffraction (XRD)

The XRD scan of *NiO* nanoparticles is shown in the Fig. 4.1. The peaks are extremely sharp due to better crystalline structure of the nanoparticles. We have found some traces of metallic Ni peaked at 44.57 Å (111) and 51.93 Å (200). The 37.36 Å, 43.34 Å, 62.90 Å and 75.35 Å are the peaks of *NiO* nanoparticles. The size of *NiO* nanoparticles is 23 nm as calculated by Debye Scherrer's formula.

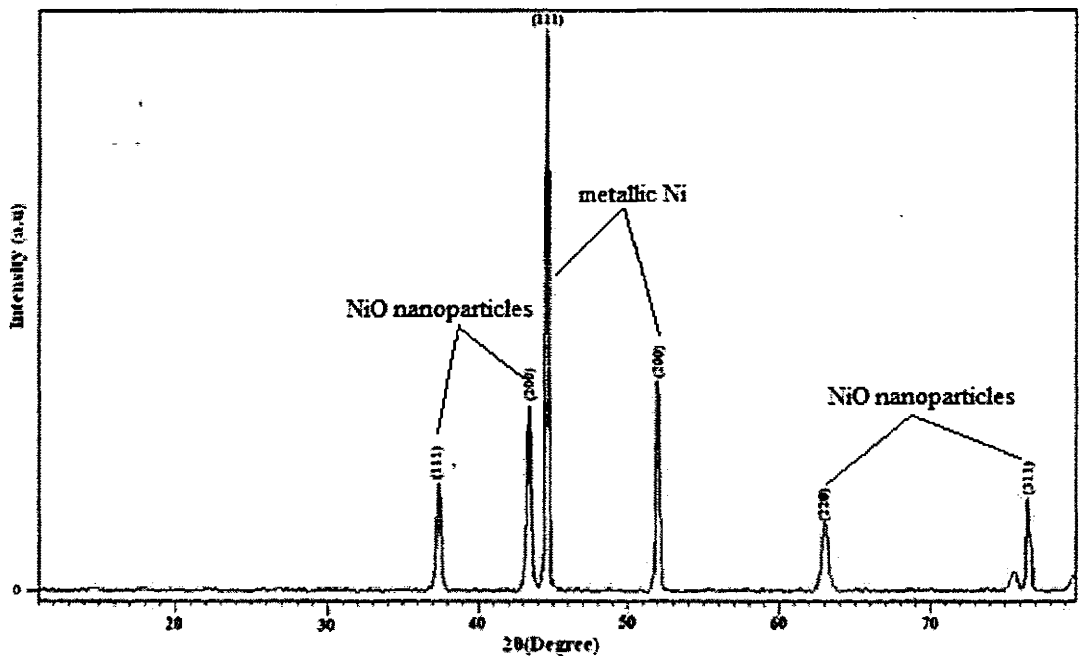


**Fig. 4.1:** XRD scan of *NiO* nanoparticles.

The XRD pattern of $(NiO)_y / Cu_{0.5}Tl_{0.5}Ba_2Ca_2Cu_3O_{10-\delta}$ $(y = 0, 0.1, 0.5 \text{ and } 2\%)$ composites is shown in the Fig. 4.2. The maximum diffraction peaks well index to tetragonal structure in P4/mmm space group. The un-doped CuTl-1223 superconductor sample is obtained by chekcell software with phase lattice parameters c = 14.21 Å and a = 4.19 Å. There is no significant effect is observed after doping of *NiO* nanoparticles on cell parameters so no stoichiometry change was observed in final compound. The c-axis length of *NiO* nanoparticles doped samples are c = 14.21 Å, 14.20 Å and 14.19 Å w.r.t wt. % 0.1, 0.5, and 2%. The slight variation of c-axis length is may be observed due to oxygen ($O_\delta$) variation in grain boundaries. Maximum peaks are obtained of our required phase CuTl-1223 superconductor but some impurity phases are also observed in XRD pattern.

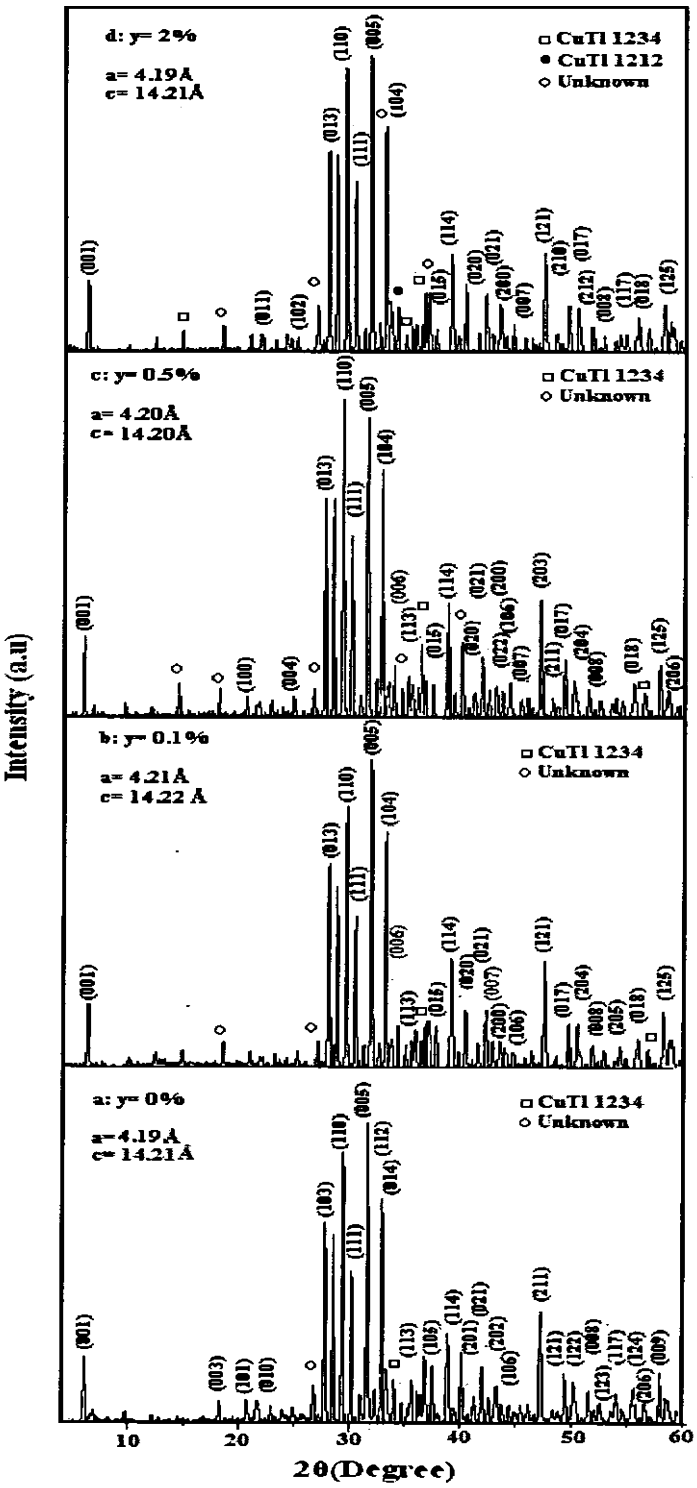


**Fig. 4.2:** XRD pattern of $(NiO)_y / Cu_{0.5}Tl_{0.5}Ba_2Ca_2Cu_3O_{10-\delta}$ superconductor composites a: y= 0%, b: y= 0.1%, c: y= 0.5%, and d: y= 2%.

## 4.3 Scanning electron microscopy (SEM)

The SEM images of $(NiO)_y / Cu_{0.5}Tl_{0.5}Ba_2Ca_2Cu_3O_{10-\delta}$ $(y = 0 \text{ and } 1\%)$ superconductor composites are shown in Fig. 4.3 (a, b).

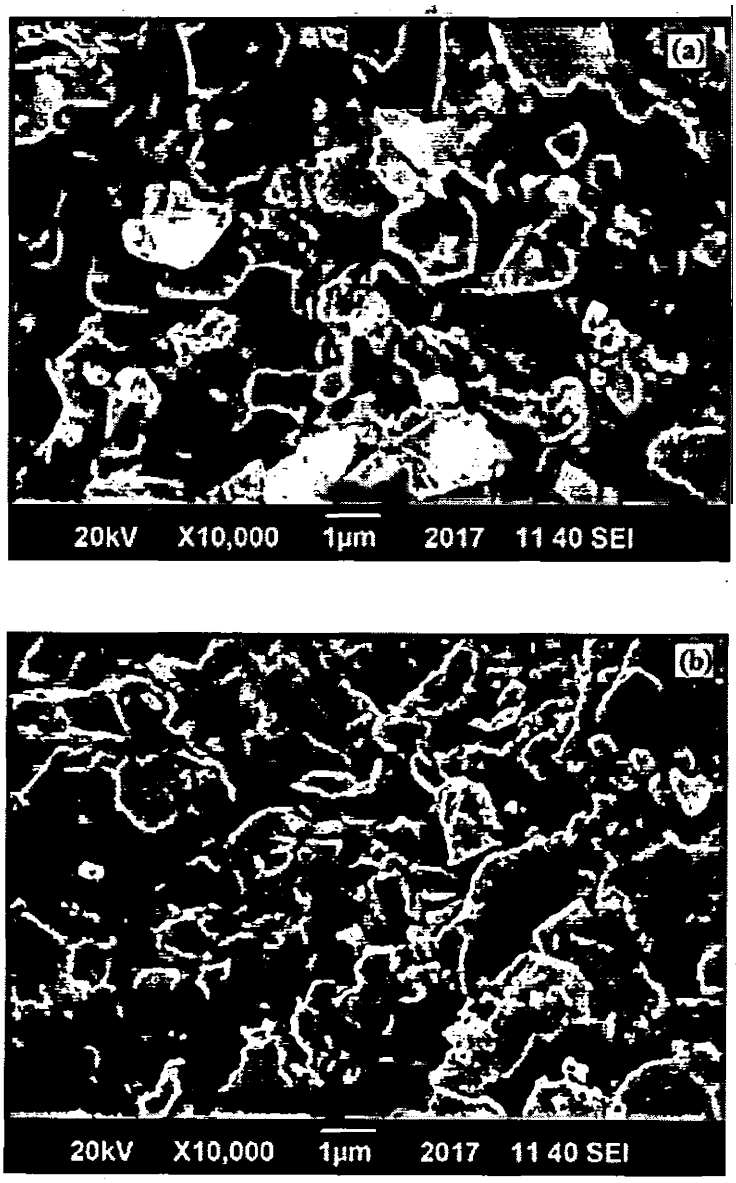


**Fig. 4.3:** (a) SEM image of $Cu_{0.5}Tl_{0.5}Ba_2Ca_2Cu_3O_{10-\delta}$ superconductor. (b) SEM image of $(NiO)_y / Cu_{0.5}Tl_{0.5}Ba_2Ca_2Cu_3O_{10-\delta}$ superconductor composite with y= 1%.

The SEM images represent the porous and granular structures in superconductor matrix. Figure 4.3 (a) clearly shows the feeble grain connectivity, high porosity and disorientation of grains in un-doped CuTl-1223 superconducting sample. Figure 4.3 (b) shows the doped sample with presence of very small percentage of *NiO* nanoparticles. This means that *NiO* nanoparticles may be present at the grain boundaries but have no large impact due to their small percentage doping.

The energy dispersive X-ray analysis (EDX) of un-doped host matrix CuTl-1223 superconductor is shown in Fig. 4.4 which clearly shows the presence of elements in a sample according to composition with minor amount of impurities (Ni and Fe).

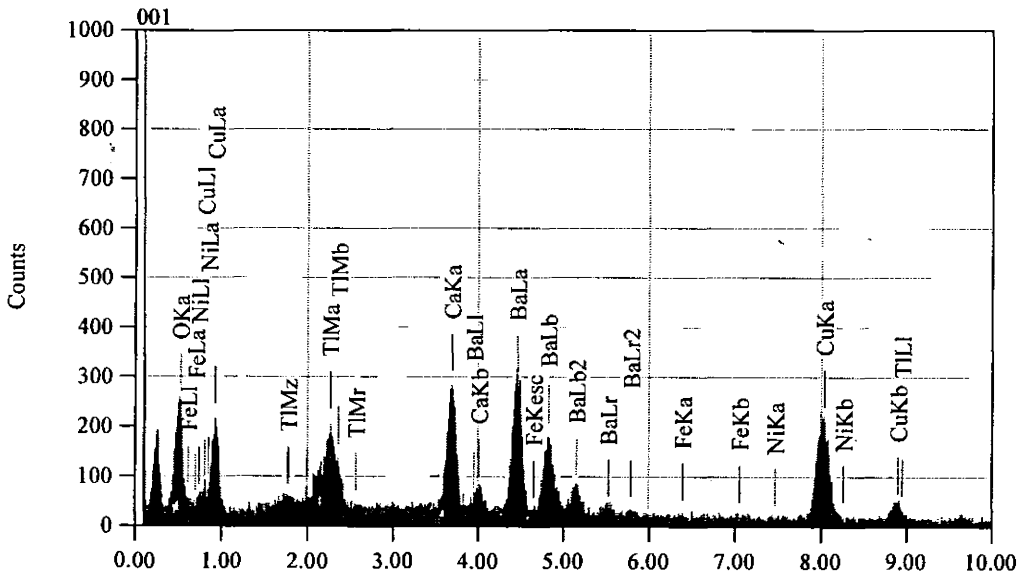


**Fig. 4.4:** EDX graph of $Cu_{0.5}Tl_{0.5}Ba_2Ca_2Cu_3O_{10-\delta}$ superconductor.

Table 4.1 shows the element composition in CuTl-1223 superconductor. It shows that CuTl-1223 as major phase with small impurities of Ni and Fe with mass percentage 0.59 and 0.23, respectively.

| Element | keV | Mass% | Error% | Atom% |
|---|---|---|---|---|
| O K | 0.525 | 11.65 | 0.68 | 40.79 |
| Ca K | 3.690 | 8.10 | 0.55 | 11.32 |
| Fe K | 6.398 | 0.23 | 1.21 | 0.23 |
| Ni K | 7.471 | 0.59 | 1.81 | 0.56 |
| Cu K | 8.040 | 33.59 | 2.37 | 29.60 |
| Ba L | 4.464 | 36.89 | 1.64 | 15.04 |
| Tl M | 2.261 | 8.94 | 1.70 | 2.45 |
| **Total** | | **100.00** | | **100.00** |

**Table 4.1:** Quantitative analysis of elements of Fig. 4.4.

## 4.4 Fourier transforms infrared spectroscopy (FTIR)

Fourier transforms infrared (FTIR) spectroscopy is the very famous spectroscopic technique used to study the local bond vibration. The formation of NiO nanoparticles has been also studied by FTIR spectroscopy.The FTIR absorption spectrum of *NiO* nanoparticles in the far-infrared region (400 – 700 $cm^{-1}$) is shown in Fig. 4.5.

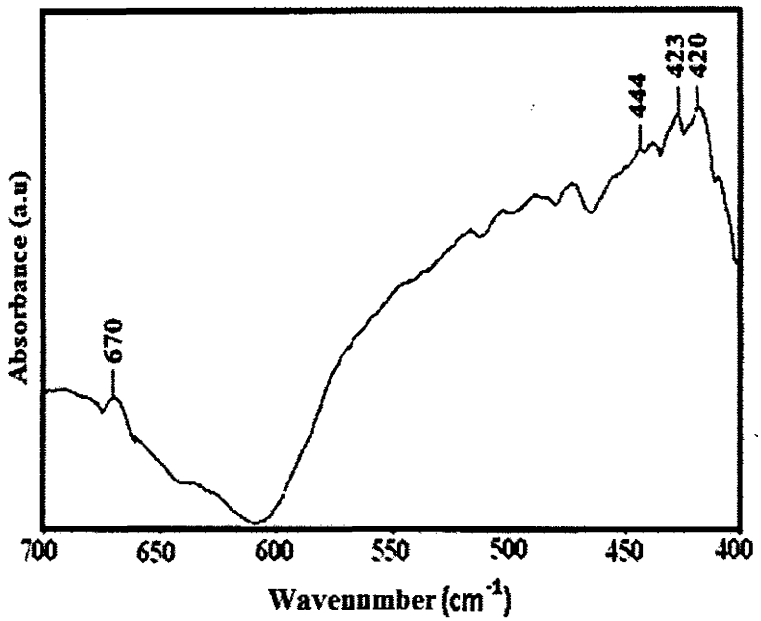


**Fig. 4.5:** Far-infrared FTIR spectrum of *NiO* nanoparticles.

The peaks within the range of 420-445 $cm^{-1}$ signify the formation of *NiO* nanoparticles. The FTIR absorption spectra of composites are used to investigate the different oxygen atoms ($O_\delta$) vibration in grain boundaries within the far-infrared range 400-700 $cm^{-1}$. The FTIR absorption spectrum of $(NiO)_y / Cu_{0.5}Tl_{0.5}Ba_2Ca_2Cu_3O_{10-\delta}$ ($y$= 0, 0.1, 0.2, 0.3, 0.4, 0.5, 1and 2%) composites are shown in Fig. 4.6 (A, B).

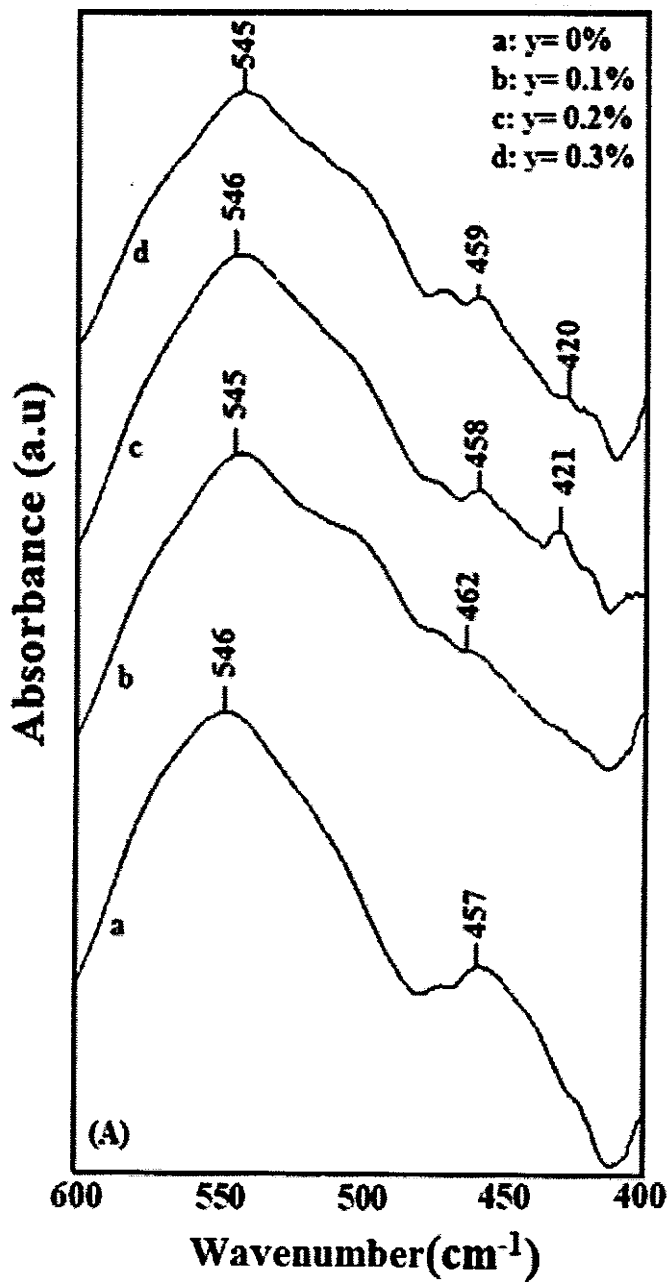
a: y= 0%
b: y= 0.1%
c: y= 0.2%
d: y= 0.3%
545
546
459
420
545
458
421
546
462
546
457
(A)
Absorbance (a.u)
600
550
500
450
400
Wavenumber(cm-1)

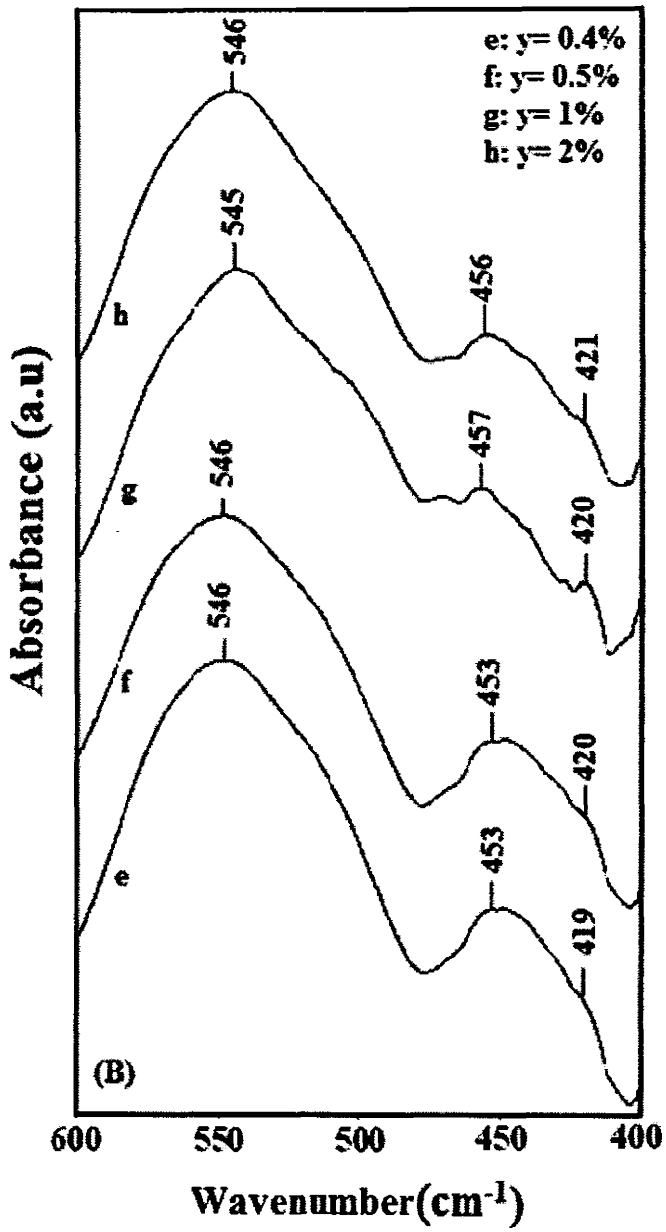


**Fig. 4.6:** (A) FTIR spectra of $(NiO)_y / Cu_{0.5}Tl_{0.5}Ba_2Ca_2Cu_3O_{10-\delta}$ a: y= 0%, b: y= 0.1%, c: y= 0.2%, and d: y= 0.3% superconductor composites, (B) FTIR spectra of $(NiO)_y / Cu_{0.5}Tl_{0.5}Ba_2Ca_2Cu_3O_{10-\delta}$ e: y= 0.4%, f: y= 0.5%, g: y= 1% and h: y= 2% superconductor composites.

The range from 400-540 $cm^{-1}$ is known as the apical oxygen atoms range and the range between 540-600 $cm^{-1}$is known as $CuO_2$ planar oxygen atoms range. The presence of vibrational bands in the range 420-445 $cm^{-1}$ confirms the presence of *NiO* nanoparticles in composite samples. The broad band in un-doped (0%) CuTl-1223 superconductor sample is observed at 546 $cm^{-1}$ and after doping of *NiO* nanoparticles it indicates almost no change between doped and un-doped samples. The increasing and decreasing effect of oxygen atoms ($O_\delta$) in composite of CuTl-1223 w.r.t wt. % (0.1, 0.2, 0.3, 0.4, 0.5, 1and 2 %) of *NiO* nanoparticles doping do not interfere in the composition but increase the intergrain coupling.

## 4.5 Resistivity measurements

The measurements of resistivity vs. temperature of CuTl-1223 superconductor samples with doping of *NiO* nanoparticles ($y$= 0, 0.1, 0.2, 0.3, 0.4, 0.5, 1and 2%) are shown in the Fig. 4.7 (a, b).

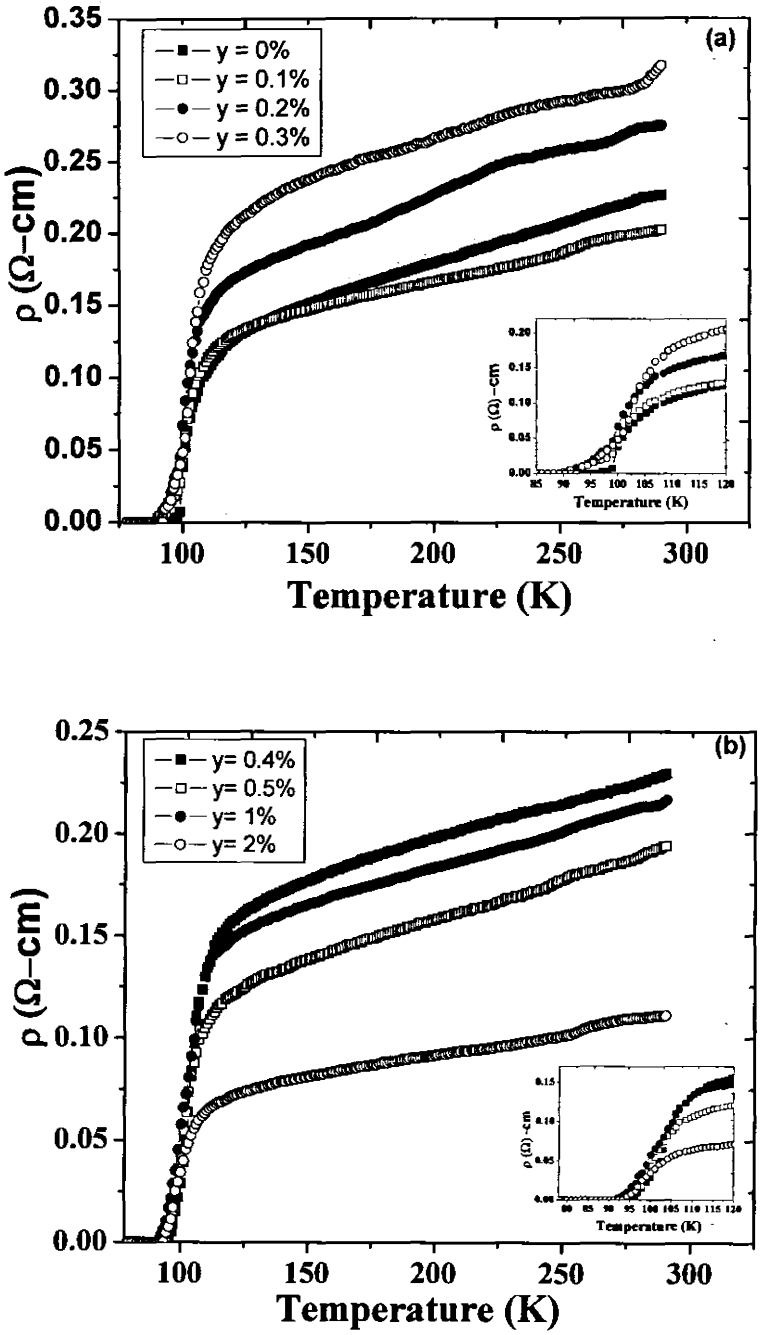


**Fig. 4.7:** (a) Resistivity vs. temperature of $(NiO)_y / Cu_{0.5}Tl_{0.5}Ba_2Ca_2Cu_3O_{10-\delta}$ ($y$= 0, 0.1, 0.2and 0.3 %) superconductor composites, (b) Resistivity vs. temperature of $(NiO)_y / Cu_{0.5}Tl_{0.5}Ba_2Ca_2Cu_3O_{10-\delta}$ ($y$= 0.4, 0.5, 1and 2 %) superconductor composites.

It can be observed from the Fig. 4.7 (a, b) that $T_c$ (R=0) of un-doped CuTl-1223 superconductor is 96 K which depressed after the doping of *NiO* nanoparticles with concentrations $y = 0.1, 0.2, 0.3, 0.4, 0.5, 1$ and 2 % with $T_c$'s 89, 91, 92, 95, 94, 91 and 93 K respectively. The decreasing $T_c$ is possibly due to the lowest porosity, trapping of mobile free carriers, accumulation of nanoparticles in grain boundaries and the variation of resistivity may also be caused due to the reflection of spin charge separation. The poor grain alignment and grain connectivity may also be gives a clue of decreasing $T_c$.

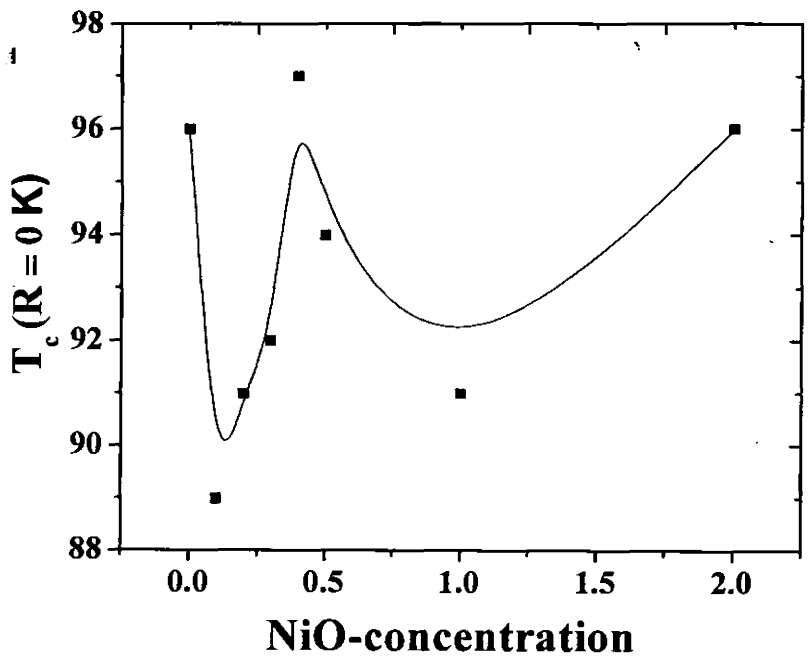


**Fig. 4.8:** The critical temperature vs. *NiO* content of $(NiO)_y / Cu_{0.5}Tl_{0.5}Ba_2Ca_2Cu_3O_{10-\delta}$ ($y = 0, 0.1, 0.2, 0.3, 0.4, 0.5, 1$ and 2%) superconductor composites.

Figure 4.8 describes the variation of $T_c$ with increasing NiO nanoparticle concentration. The fluctuation in critical temperature with different concentration of *NiO*

nanoparticles may be due to poor homogeneous distribution of carriers, impurities phase's composition variation and disorientation of grain boundaries.

## 4.6 AC susceptibility measurements

The magnetic susceptibility in-phase component ($\chi'$) represents the volume fraction, magnetic response and out-phase component ($\chi''$) represents the energy loses due to weak intergrain links. The AC susceptibility versus temperature measurement of the samples y= 0, 0.1, 0.2 and 0.3% is shown in Fig. 4.9.

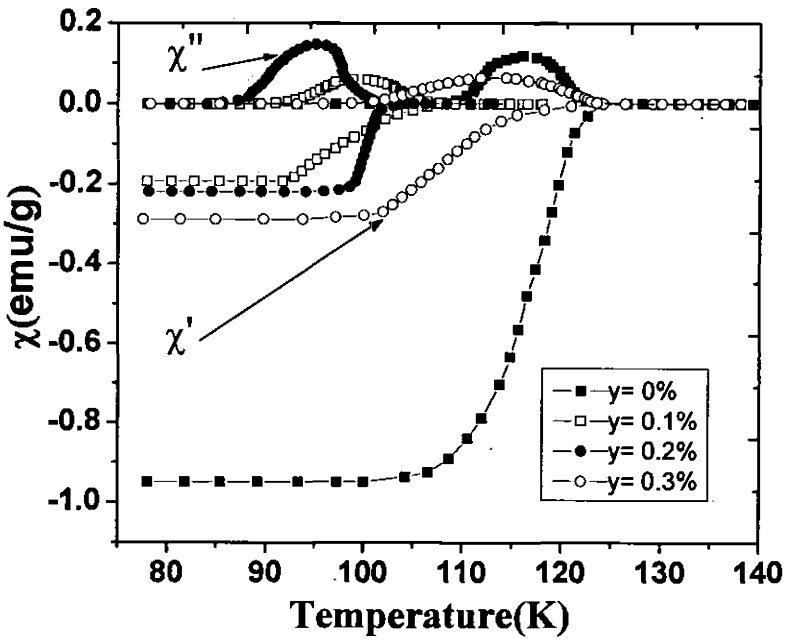


**Fig. 4.9:** The ACsusceptibility vs. temperature measurements of $(NiO)_y / Cu_{0.5}Tl_{0.5}Ba_2Ca_2Cu_3O_{10-\delta}$ ($y = 0, 0.1, 0.2$ and 0.3%) superconductor composites.

The magnitude of diamagnetism in $(NiO)_y$ /CuTl-1223 $y = 0, 0.1, 0.2$ and 0.3% composite samples is suppressed due to the doping concentration of $NiO$ nanoparticles which

deprave the superconductivity. The decrease in diamagnetic behavior of the composite is due to antiferromagnetic $NiO$ nanoparticles which has a small net magnetic moment due to uncompensated surface spins on individual nanoparticle surface. Therefore fluctuation of diamagnetism was observed in $NiO$ nanoparticles doped samples.

## 4.7 Conclusion

We have synthesized the NiO nanoparticles and $(NiO)_y / Cu_{0.5}Tl_{0.5}Ba_2Ca_2Cu_3O_{10-\delta}$ (y=0, 0.1, 0.2, 0.3, 0.4, 0.5, 1 and 2%) nanoparticles/superconductor composites by sol-gel method and solid-state reaction method, respectively. The structural and physical properties have been examined by X-ray diffraction (XRD), Scanning electron microscopy (SEM), Energy dispersive X-ray (EDX) analysis, Fourier transforms infrared (FTIR) spectroscopy, Resistivity, and AC susceptibility techniques. The *NiO* nanoparticles have cubic structure and superconductor matrix has tetragonal structure, which is obtained by XRD technique. There is no change observed in cell parameters with the increased *NiO* nanoparticles doping concentration. The size of *NiO* nanoparticles is calculated by Debye Scherrer's formula which is 23 nm. The granular structure of the host CuTl superconducting matrix has been confirmed by SEM images and EDX shows the elemental composition of CuTl-1223 superconductor. The FTIR measurement confirms the formation of *NiO* nanoparticles and their presence in the composites. FTIR spectroscopy suggests that the doping of *NiO* nanoparticles do not interacts with host superconductor matrix and lies between grain boundaries. The critical temperature and magnitude of diamagnetism are decreased with increased *NiO* nanoparticles concentration. The most probable reasons of depression of superconducting properties due to doping of *NiO* nanoparticles in host CuTl superconductor matrix is trapping of mobile free carriers, spin-spin interaction and poor grain connectivity and porosity. The decreasing magnitude of diamagnetism in AC susceptibility is appeared due to antiferromagnetic behavior of *NiO* nanoparticles.

# References

[1] C. Kittel, Introduction to Solid State Physics,seventhedition,John Wiley & Sons (2004).

[2] J. J. Powell, N. Faria, E. Thomas-Mckay, and L. C. Pele, J Autoimmunity **34**, J226-J233 (2010).

[3] S. K. Sahoo, S. Parveen, and J. J. Panda, Nanomedicine, **3**, 20-31 (2007).

[4]V.V. Schmidt; P. Muller, A. V. Ustinov (eds); The Physics of Superconductors: introduction to fundamentals and applications, Springer- Verlag Berlin Heidelberg, New York (1997).

[5]U.S. Congress, Office of Technology Assessment, High-Temperature Superconductivity in Perspective, OTA-E-440, Washington, DC: U.S. Government Printing Office, April (1990).

[6] C. Buzea, and K. Robbie, Superconductivity. Sci. Technol. **18**, R1 (2005).

[7] P. W. Philips, Advanced Solid State Physics, Westview Press(2003).

[8] R. A. Shukor, High Temperature Superconductors: Materials Mechanisms and Applications, Akademi Sains, Malaysia (2009).

[9] W. Meissner, and R. Oschsenfeld, Naturwissen Schafttes **21**, 787 (1933).

[10] H. K. Onnes, Akad.Van. Wetenschappen (Amsterdam) **14**, 113, 818 (1911).

[11] M. S. Vijaya, Materials Science, McGraw-Hill Publishing Company Limited, p: 323, 324 (2003).

[12] F, and H. London, Proceedings of the Royal Society of London, **A149**, 71 (1935).

[13] J. F. Annett, Superconductivity, Superfluids and Condensates, Oxford University Press, p: 67 (2004).

[14] V. L. Ginzburg, and L. D. Landau, Zh. Eksperim. i Teor. Fiz.**20**, 1064(1950).

[15] J. Bardeen, L. N. Cooper, and J. R. Schrieffer, Phys. Rev. **108**, 1175 (1957).

[16] B. D. Josephson, "Possible new effects in superconductive tunneling",Physics letters **1(7)**: 251-253 (1962).

[17] H. Ibach, and H. Luth, Solid State Physics: An Introduction to Theory and Experiment, Springer-Verleg (1991).

[18] M. Tinkham, Introduction to Superconductivity, second edition, McGraw-Hill, Inc, New York.

[19] M. K. Wu, J. R. Ashburn, C. J. Trong, P. H. Hor, R. L. Meng, L. Gao, Z. J. Hung, Y. Q. Wang, and C. W. Chu, Phys. Rev. Lett. **59**, 908 (1987).

[20] C. Michel, M. Hervieu, M. M. Borel, A. Grandin, F. Deslandes, J. Provost, and B. Raveau, Z. Phys. B **68**, 421 (1987).

[21] Y. Muraoka, M. Kikuchi, N. Ohnishi, K. Hiraga, R. Suzuki, N. Kobayashi, and Y. Syono, Physica C **204**, 65 (1992).

[22] S. Adachi, H. Yamauchi, S. Tanaka, and N. Mori, Physica C**212**, 164 (1993).

[23] M. Kikuchi, T. Kajitani, T. Suzuki, S. Nakajima, K. Hiraga, N. Kobayashi, H. Iwasaki, Y. Syono, and Y. Muto, Jpn. J. Appl. Phys. **28**, L382 (1989).

[24] S. S. P. Parkin, V. Y. Lee, E. M. Engler, A. I. Nazzal, T. C. Huang, G. Gormau, R. Savoy, and R. Beyer, Phys. Rev. Lett. **60**, 2539 (1988).

[25] C. Martin, C. Michel, A. Maignan, M. Hervieu, and B. Raveau, C. R. Acad. Sci. Ser.2, **307**, 27 (1988).

[26] H. Ihara, K. Tanaka, Y. Tanaka, A. Iyo, N. Terada, M. Tokumoto, M. Ariyama, I. Hase, A. Sundaresan, N. Hamada, S. Miyashita, K. Tokiwa, and T. Watanabe, Physica C **341**, 487 (2000).

[27]C.Kittel, Introduction to Solid State Physics John Wiley & Sons. pp. 273–278 (2004).

[28] A. A. Abrikosov: Zh. Eksp. Teor, English transl, Sov. Phys. JETP **5**, 1174 (1957).

[29] M. A. Omar, Elementary Solid State Physics,thirdedition, (2007).

[30] L. Cooper Physical Review **104**, 1189-1190 (1956).

[31] Introduction to Superconductivity,second edition, A. C. Rose Innes and E. H. Rhoderick, Pergamon Press, Oxford UK (1969).

[32] V. V. Schmidt, the Physics of Superconductors, Nauka Publishers, Moskaue, p: 1 (1982).

[33] Rohlf, James William, ch 15 Modern Physics, Johns Wiley (1994).

[34] S. O. Pillai, Solid State Physics, fifth edition, New Age International (p), Limitted Publishers (2002).

[35] H. Ihara, K. Tokiwa, H. Ozawa, M. Hirabayashi, A. Negishi, H. Matuhata, and Y.S. Song, Jpn. J. Appl. Phys. **33**, L503 (1994).

[36] Z. Z. Sheng, and A. M. Hermann, Nature **332**, 138 (1988).

[37] G. Malandrino, D. S. Richeson, T. J. Marks, D. C. De Groot, J. L. Schindler, and C. R. Kannewurf, Appl. Phys. Lett. **58**, 182 (1991).

[38] M. Kikuchi, T. Kajitani, T. Suzuki, S. Nakajima, K. Hiraja, N. Kobayashia, H. Iwasaki, Y. Syono, and Y. Muto, Jpn. J. Appl. Phys. **28**, L382 (1989).

[39] S. S. P. Parkin, V. Y. Lee, E. M. Engler, A. I. Nazzal, T. C. Huang, G. Gormau, R. Savoy, and R. Beyer, Phys. Rev. Lett. **60**, 2539 (1988).

[40] M. Karppinen, H. Yamauchi, Y. Morita, M. Kitabatake, T. Motohashi, R. S. Liu, J. M. Lee, and J. M. Chen, Journal of Solid State Chemistry **177**, 1037 (2004).

[41] H. Ihara, Physica C **364**, 289 (2001).

[42] K. Semba, A. Matsuda, and T. Ishii, Phys. Rev. B**49**, 10043 (1994).

[43] K. Tokiwa, H. Aota, C. Kunugi, K. Tanaka, Y. Tanaka, A. Iyo, H. Ihara, and T. Watanabe, Physica B **284**, 1077 (2000).

[44] K. Tanaka, A. Iyo, N. Terada, K. Tokiwa, S. Miyashita, Y. Tanaka, T. Tsukamoto, S. K. Agarwal, T. Watanabe, and H. Ihara, Phys. Rev. B **63**, 064508 (2001).

[45] T. Shibata, T. Tatsucki, S. Adachi, K. Tanabe, S. Fujihara, and T. Kimura, Physica C **353**, 200 (2001).

[46] M. S. Vijaya, Materials Science, McGraw-Hill Publishing Company Limited, p: **352-354** (2003).

[47] L. P. Balogh, Nanomedicines, Nanotechnology, Biology and Medicines **6**, 397-398 (2010).

[48] F. Sanchez, K. Sobolev, Construction and Building Materials **24**, 2060-2071 (2010).

[49] Nanotechnology for Dummies, second edition, John Wiley & Sons (2011).

[50] G. Cao, Nanostructures and Nanomaterials, Imperial College Press, London(2004).

[51] N. C. Mueller, and B. Nowack, Elements **6**, 395-400 (2010).

[52] R. H. Kodama, and J. Magn Mater**200**, 359 (1999).

[53] C. Luna, M. P. Morales, C. J. Serna, and M. Vázquez, Nanotechnology **14**, 268 (2003).

[54] Silver nanoparticles Properties, Characterization and Applications, Nova Science Pub Incorporated (2010).

[55] R. F. Service, Science **293**, 782 (2001).

[56] C.A. Haberzettl, Nanotechnology **13**, R9 (2002).

[57] T.A. Taton, Nature Muter**2**, 73 (2003).

[58] J.J. Storhoff, R. Elghanian, R.C. Mucic, C.A. Mirkin, and R.L. Letsinger, J: Am. Chem. Soc. **120**, 1959 (1998).

[59] G.C. Bond, Cutal. Today **72**, 5 (2002).

[60] R. Dingle, W. Wiegmann, and C.H. Henry, Phys. Rev. Lett. **33**, 827 (1974).

[61] W. Zhang, J Nanoparticle Research **5**: 323-332 (2003).

[62] T. Hyeon, The Royal Society of Chemistry, 927-934 (2003).

[63] M. S. Vijaya, Materials Science, McGraw-Hill Publishing Company Limited, p: 528, 529 (2003).

[64] I. Karaca, O. Uzun, U. Kölemen, F. Yılmaz, and O. Sahin, JAlloys Compd. 476, 486 (2009).

[65] M. Daumling, J.C. Grivel, B. Hensel, and R. Flukiger, Physica C **219**, 429 (1994).

[66] S. A. Sergeenkov, Physica C **205**, 1-13 (1993).

[67] N.A. Khan, A.A. Khurram, Appl. Phys. Lett. **86**, 152502 (2005).

[68] E.Guilmeau, B. Andrzejewski, and J.G. Noudem. Physica C **387**, 382 (2003).

[69] N. H. Mohammed, A. I. Abou-Aly, I. H. Ibrahim, R. Awad, and M. Rekaby, J Alloys and Compounds **486**, 733-737 (2009).

[70] A. Ghattas, M. Annabi, M. Zouaoui, F. B. Azzouz, and M. B. Salem, Physica C **468**, 31-38 (2008).

[71] M. M. Elokr, R. Awad, A. A. El-Ghany, A.A. Shama, and A. A. El-wanis, J Superconductor Nov Magn (2010).

[72] M. Farbod, and M. R. Batvandi, Physica C **471**, 112-117 (2011).

[73] N. H. Mohammed, A. I. Avou-Aly, I.H. Ibrahim, R. Awad, and M. Rekaby, J Superconductor Nov Magn (2010).

[74] Y.Moritomo, Y. Tomioka, A.Asamitsu, Y. Tokura, and Y. Matsui, Phycica B **51**, 5 (1995).

[75] H. Yamauchi, M. Karppinen, and S.Tanaka, Phycica C **263**, 146-150 (1996).

[76] V. F. Masterov, N. M. Shibanova, and K. F. Shtel'makh Zh, Tekh. Fiz **67**, 137-138 (1997).

[77] S. K. Agarwal, A. Iyo, K. Tokiwa, Y. Tanaka, K. Tanaka, M. Tokumoto, N. Terada, T. Saya, M. Umeda and H, Ihara, Physical Review B **58**, 14 (1998).

[78] H. Ihara, Y. Sekita, H. Tateai, N. A. Khan, K. Ishida, E. Harashima, T. Kojima, H. Yamamoto, K. Tanaka, Y. Tanaka, N. Terada, and H. Obara, IEEE Transations on Applied Superconductivity **9**, 1551-1554 (1999).

[79] K. Tanaka, A. Iyo, Y. Tanaka, K. Tokiwa, N. Terada, M. Tokumoto, M. Ariyama, T. Tsukamoto, S. Miyashila, T. Watanabe, and H. Ihara, Physica B **284**, 1079 (2000).

[80] E. Kuzmann, W.T Konig, M.Mair, Z. Homonnay, Z. Klencsar, G. Juhasz, and G.Gritzner, Superconductor. Sci. Technol **14**, 379-385 (2001).

[81] K. Christova , A. Manov, J. Nyhus, U. Thisted, O. Herstad, S.E. Foss, K.N. Haugen, and K. Fossheim, J Alloys and Compounds **340**, 1–5 (2002).

[82] S. X. Dou, W. K. Yeoh, J. Horvat, and M. Ionescu, Applied Phys. Lett. **83**, 24 (2003).

[83] Y. Ichiyanagi, N. Wakabayashi, J. Yamazaki, S. Yamada, Y. Kimishima, E. Komatsu, and H. Tajima, Physica B **329-333**, 862-863 (2003).

[84] S. Chkoundali, S. Ammar, N. Jouini, F. Fievet, P. Molinie, M. Danot, F. Villain, and J-M Greneche, J. Physics Condens. Matter **16**, 4357-4372 (2004).

[85] S. Y. Xie, Z. J. Ma, C. F. Wang, S. C. Lin, Z. Y. Jiang, R. B. Huang, and L. S. Zehang, J. Solid State Chem. **177**, 3743 (2004).

[86] M. Ghosh, K. Biswas, A. Sundaresan, and C. N. R. Rao, J. Mate Chem **16**, 106-111 (2005).

[87] I. E. Agranovski, A. Y. Ilyushechkin, I. S. Altman, T. E. Bostrom, and M. Choi, Physica C **434**, 115–120 (2006).

[88] Q. Li, L. Wang, B. Hu, C. Yang, L. Zhou, and L. Zhang, Material Letters **61**, 1615-1618 (2007).

[89] Y. Xu, A. Hu, C. Xu, N. Sakai, I. Hirabayashi and M. Izumi, Physica C **468**, 1363–1365 (2008).

[90] N. H. Mohammed, A. I. Abou-Aly, I. H. Ibrahim, R. Awad, and M. Rekaby, J Alloys and Compounds 486 (2009).

[91] M. M. Elokret, R. Awad, A. A. El-Ghany, A. A. Shama, and A. El-wanis, J Superconductor Nov Magn (2010).

[92] M. M. K. Motlagh, A. A. Youzbashi, and L. Sabaghzadeh, International J Physical Sciences **6**, 1471-1476 (2011).

[93] N. A. Khan, A. Saleem, and S. T. Hussain, J Superconductor Nov Magn (2012).

[94] C. N. R. Rao, Phil. Trans. R. Soc. A**336**, 595 (1991).

[95] C. N. R. Rao, and J. Gopalakrishnan, New Directions in Solid State Chemistry, Cambridge: Cambridge University Press(1989).

[96] B. D. Cullity, Elements of X-ray Diffraction, Addison-Wesley Publishing Company, Inc. (1956).

[97] C. Giacovazzo, Fundamentals of Crystallography,second edition, Oxford science publications(2002).

[98] B. E. Warren, X-ray Diffraction, General publishing company (1969).

[99] L. Alexander, and H. P. Klug, J. App. Physics **21**, 126 (1950).

[100]S. Amelinckx, D. V. Dyck, J. V. Landuyt, and G. V. Tendeloo, Handbook of Microscopy Methods II, (1997).

[101] N. Hassan, PhD Thesis, Solid state synthesis and studies of Ni doped superconductor, Material Science Laboratory, QAU 2009.

[102] M. Mumtaz, PhD Thesis,Synthesis and characterization of $Cu_{0.5}Tl_{0.5}Ba_2Ca_{n-1}Cu_{n-y}Zn_yO_{2n+4-\delta}$ ($n$ = 3, 4) High temperature superconductors Material Science Laboratory, QAU 2008.

[103] H. Ibach, and H. Luth, Solid State Physics: An Introduction to Theory and Experiment,Springer-Verleg(1991).

[104] M. Nikolo Am. J. Physics **63**, 57-65 (1995).

[105] M. I. Youssif, A. A. Bahgat, and I. A. Ali, Egypt. J. Sol., Vol **23**(2000).

[106] H. Ihara, A. Iyo, K. Tokiwa, K. Ishida, N. Terada, M. Tokumotu, Y. Sekita, T. Tsukamoto, T. Watanabe, and M. Umeda, Physica C, 282-287 (1997).

[107] P. Zoller, J. Glaser, A. Ehmann, C. Schultz, W. Wischert, S. Kemmler-Sack, T. Nissel, and R. P. Huebener, Z. Phys. B **96**, 505(1995).

[108] Jin-Tae Kim, T. R. Lemberger, S. R. Foltyn, and X. Wu, Phys. Rev. B **49**, 15970 (1994).

[109] D. A. Bonn, S. Kamal, K. Zhang, R. Liang, D. J. Baar, E. Klein, and W. N. Hardy, Phys. Rev. B **50**, 4051 (1994).

[110] V. Bartunek, and O. Smrckova, Ceramics-Silikaty **54**, 133-138 (2010).

[111] S. X. Dou, S. Soltanian, J. Horvat, X. L. Wang, P. Munroe, S. H. Zhou, M. Ionescu, H. K. Liu, and M. Tomsic, Apllied Physics Letters **81**, 18 (2002).

[112] M. Annabi, A. M_chirgui, F. Ben Azzouz, M. Zouaoui, and M. Ben Salem, Physica C **405**, 25–33 (2004).

[113] S. X. Dou, S. Soltanian, Y. Zhau, E. Getin, Z. Chen, O. Shcherbakoba, and J. Horvat, Superconductor. Sci. Technol, **18**, 710-715 (2005).

[114] C. Xu, A. Hu, M. Ichihara, N. Sakai, I. Hirabayashi, and M. Izumi Physica C **460–462**, 1341–1342 (2007).

[115] R. Awad, Superconductor Nov Magn **21**, 461-466 (2008).

[116] M. Mumtaz, and N. A. Khan, Phys. Scr. **80** (2009).

[117] B. A. Albiss, I. M. Obaidat, M. Gharaibeh, H. Ghamlouche and S. M. Obeidat, Solid State Communications **150**, 1542-1547 (2010).